Pharmacological Research 197 (2023) 106968

Contents lists available at ScienceDirect

Pharmacological Research

journal homepage: www.elsevier.com/locate/yphrs

Penicopeptide A (PPA) from the deep-sea-derived fungus promotes osteoblast-mediated bone formation and alleviates ovariectomy-induced bone loss by activating the AKT/GSK-3β/β-catenin signaling pathway

Chun-Lan Xie [a,b,1], Yu-Ting Yue [a,d,1], Jing-Ping Xu [a], Na Li [a], Ting Lin [e], Guang-Rong Ji [d,*], Xian-Wen Yang [b,*], Ren Xu [a,c,**]

[a] Fujian Provincial Key Laboratory of Organ and Tissue Regeneration, School of Medicine, Xiamen University, Xiamen 361102, China
[b] Key Laboratory of Marine Genetic Resources, Third Institute of Oceanography, Ministry of Natural Resources, Xiamen 361005, China
[c] The First Affiliated Hospital of Xiamen University-ICMRS Collaborating Center for Skeletal Stem Cells, State Key Laboratory of Cellular Stress Biology, Faculty of Medicine and Life Sciences, Xiamen University, Xiamen 361102, China
[d] Department of Orthopedics Surgery, Xiang'an Hospital of Xiamen University, School of Medicine, Xiamen University, 361102, Xiamen,China
[e] Fujian Provincial Key Laboratory of Innovative Drug Target Research, School of Pharmaceutical Sciences, Xiamen University, Xiamen 361102, China

ARTICLE INFO

Keywords:
Osteoporosis
Osteoblasts
Penicopeptide A
Marine natural product
AKT/GSK-3β/β-catenin

Chemical compounds studied in this article:
Viridicatol (PubChem CID: 115033)
Viridicatin (PubChem CID: 67206)
(−)-Cyclopenol (PubChem CID: 16681741)
(−)-Solitumidines D (PubChem CID: 155552764)
Solitumine A (PubChem CID: 155537754)
Indole-3-acetic acid methyl ester (PubChem CID: 74706)
Hydroxypropan-2'
3'-diol orsellinate (PubChem CID: 71501072)

ABSTRACT

The potential of marine natural products as effective drugs for osteoporosis treatment is an understudied area. In this study, we investigated the ability of lead compounds from deep-sea-derived *Penicillium solitum* MCCC 3A00215 to promote bone formation in vitro and in vivo. We found that penicopeptide A (PPA) promoted osteoblast mineralization among bone marrow mesenchymal stem cells (BMSCs) in a concentration-dependent manner, and thus, we selected this natural peptide for further testing. Our further experiments showed that PPA significantly promoted the osteogenic differentiation of BMSCs while inhibiting their adipogenic differentiation and not affecting their chondrogenic differentiation. Mechanistic studies showed that PPA binds directly to the AKT and GSK-3β and activates phosphorylation of AKT and GSK-3β, resulting in the accumulation of β-catenin. We also evaluated the therapeutic potential of PPA in a female mouse model of ovariectomy-induced systemic bone loss. In this model, PPA treatment prevented decreases in bone volume and trabecular thickness. In conclusion, our in vitro and in *vivo* results demonstrated that PPA could promote osteoblast-related bone formation via the AKT, GSK-3β, and β-catenin signaling pathways, indicating the clinical potential of PPA as a candidate compound for osteoporosis prevention.

Abbreviations: PPA, penicopeptide A; BMSCs, bone mesenchymal stem cells; BMMs, bone marrow monocytes; MNPs, marine natural products; Runx2, Runt-related transcription factor 2; ALP, alkaline phosphatase; Ibsp, integrinbinding sialoprotein; HIVEP3, human immunodeficiency virus type I enhancer binding protein 3; OCN/Bglap, osteocalcin; GSK-3β, glycogen synthase kinase-3; p-GSK-3β, phosphorylated glycogen synthase kinase-3; AKT, protein kinase B; p-AKT, phosphorylated protein kinase B; DMSO, dimethyl sulfoxide; PBS, phosphate-buffered saline; RT-qPCR, quantitative polymerase chain reaction; TGF-β, transforming growth factor beta; MAPK, mitogen-activated protein kinase; PI3K, phosphatidylinositol 3-kinase complex; P38 MAPK, p38 mitogen-activated protein kinases; GAPDH, glyceraldehyde-3-phosphate dehydrogenase; MTT, 3-(4,5-Dimethylthiazol-2-yl)− 2,5-diphenyltetrazoliumbromide; EC_{50}, concentration for 50% of maximal effect; OVX, ovariectomy; NC, control; Diff., PM, differentiationPurmorphamine; EDTA, ethylene diamine tetraacetic acid; α-MEM, α Minimum Essential Medium; FBS, fetal bovine serum; FFA, free fatty acid; pNPP, phosphatase substratenitrophenol phosphate; TGF-β3, transforming growth factor beta 3; cDNA, complementary DNA; PCA, principal component analysis; GO, gene Ontology; KEGG, kyoto encyclopedia of genes and genomes; BSA, bovine serum albumin; DAPI, 4', 6-diamidino2-phenylindole; μCT, high-resolution micro–computed tomography; BV/TV, bone volume/tissue volume; Tb.Th, trabecular thickness; Tb.Sp, trabecular separation; Tb.N, trabecular number; Cs.th, cross-sectional thickness; Ob.S/BS, osteoblast surface/bone surface; N.Oc./B.Pm, osteoclast number; MS/BS, mineralizing surface/bone surface; MAR, mineral apposition rate; BFR/BS, bone formation rate/bone surface; OD, optical density; RNA-seq, RNA-sequencing; OCT, optimal cutting temperature compound.

* Corresponding authors.
** Corresponding author at: Fujian Provincial Key Laboratory of Organ and Tissue Regeneration, School of Medicine, Xiamen University, Xiamen 361102, China.
E-mail addresses: jiguangrong@sina.cn (G.-R. Ji), yangxianwen@tio.org.cn (X.-W. Yang), xuren526@xmu.edu.cn (R. Xu).
[1] These authors contributed equally to this work

https://doi.org/10.1016/j.phrs.2023.106968
Received 11 July 2023; Received in revised form 19 October 2023; Accepted 19 October 2023
Available online 20 October 2023

mL-236A (PubChem CID: 173651)
(*R*)-Mevalonolactone (PubChem
CID: 6419891)
Solitumidine A (PubChem CID: 155529073)

1. Introduction

Obesity and osteoporosis have become major global health problems in recent decades, as their prevalence rates have continually increased [1]. Emerging data have given rise to the hypothesis that bone marrow rich in fat may be responsible for osteoporosis. This phenomenon is frequently observed in systemic adiposity as well as osteoporosis, especially in postmenopausal women. [2,3] Both osteoblasts, which function in bone metabolism, and adipocytes, which are responsible for fat metabolism, differentiate from bone marrow mesenchymal stem cells (BMSCs), and a trade-off exists between osteoblast and adipocyte formation. A decrease in bone mass is often accompanied by an increase in the fat content within the marrow cavity [4–6]. When the balance of lipid metabolism is disrupted, abnormal bone metabolism also occurs, which can then lead to bone metabolism-related diseases. Conversely, several skeletal diseases, including bone loss and osteoarthritis, are commonly accompanied by hyperlipidemia, fatty liver, and lipid metabolism-related diseases. Together these findings in the literature indicate that a close relationship exists between bone metabolism and fat metabolism. Therefore, bone regeneration through directional induction of BMSCs is expected to promote osteogenesis and provide a rational therapeutic strategy for preventing age-related osteoporosis [7].

Marine natural products (MNPs) have shown various potent biological effects against numerous diseases, especially different cancers and infectious diseases [8,9]. Currently, MNP-based drugs approved by the Food and Drug Administration include ziconotide, cytarabine, and trabectedin. While MNPs have greatly contributed to the discovery and development of new drugs, only rare MNPs that induce osteoblast differentiation (e.g., hymenialdisine, phorbasone A, phorbasone B, phorboketal A, majusculamide A, and majusculamide B) have been reported. Furthermore, fewer osteoblast differentiation promotors have been isolated from natural sources relative to osteoclast differentiation inhibitors [10]. Therefore, the identification of bioactive small molecules within MNPs that can regulate the fate of BMSCs represents a new direction in the search for anti-osteoporosis candidate drugs.

In our previous study, 18 tetracyclic steroids bearing a bicyclo[4.4.1] ring system were obtained from the deep-sea-derived fungus *Rhizopus* sp. W23 and found to act as potent antiosteoporosis agents. Among them, neocyclocitrinol C significantly enhanced osteoblastogenesis and inhibited adipogenesis in BMSCs, indicating the potential of MNPs as anti-osteoporosis drug leads [11]. In our another study, 25 compounds were isolated from the deep-sea-derived *Penicillium solitum* MCCC 3A00215 [12]. To advance this line of research, the present study tested the anti-osteoporosis activities of these compounds among BMSCs and the MC3T3-E1 osteoblast line in vitro as well as in an ovariectomy (OVX) mouse model in vivo to determine if they offer a preventive effect on estrogen deficiency-induced bone loss.

2. Materials and methods Materials and methods

2.1. Reagents and antibodies

Alpha-modified minimal essential medium (α-MEM), fetal bovine serum (FBS), and penicillin/streptomycin were purchased from Gibco (Carlsbad, CA, USA). β-Glycerophosphate (S0942), DMSO (34869), Alizarin red S (A5533), and oil red O were provided by Sigma (Saint Louis, Missouri, USA). Ascorbic acid (60374ES60) was obtained from Yeasen (Shanghai, China). β-Catenin (15B8, 1:1000), GSK-3β (D5C5Z, 1:1000), phospho-GSK-3β (Ser9) (D3A4, 1:1000), AKT (C67E7, 1:1000), phospho-AKT (Ser473) (D9E, 1:2000), and GAPDH (D4C6R, 1:1000) antibodies were obtained from Cell Signaling Technology (Boston, USA). An OCN antibody was purchased from Abcam (ab93876, 1:200, Cambridge, UK). Rabbit/mouse HRP-conjugated secondary antibodies were all obtained from LABLEAD (S0101 and S0100; 1:5000, Beijing, China). Alexa Fluor 594 donkey anti-mouse IgG (H+L) (A11032, 1:400 dilution), Alexa Fluor 488 donkey anti-rabbit (H+L) (A21206, 1:400 dilution), and DAPI (0.1 μg/mL, 1:10000) were obtained from Invitrogen by Thermo Fisher Scientific (Waltham, MA, USA). Vazyme's HiScript II Q RT SuperMix (R22301), TRIzol (R40101AA), and ChamQ Universal SYBR qPCR Master Mix (Q71102) were purchased from Vazyme (Nanjing, China). Cellcook provided the Cell Counting Kit-8 (CCK-8, CT01A, Guangzhou, China). A micromethod triglyceride (TG) content assay kit (D799796–0100) and free fatty acid (FFA) content assay kit (D799794–0100) were obtained from Sangon Biotech (Shanghai, China). The sequences of the primers used in RT–qPCR were provided by Origene (Maryland, USA). Chloroform, isopropanol, ethanol, and other organic reagents were all obtained from Sinopharm (Beijing, USA). All antibodies were monoclonal antibodies. Akt1 (NM_009652) mouse recombinant protein (TP507696, Maryland, USA) and mouse GSK-3β protein (MCE, HY–P73090, New Jersey, USA) were obtained from Origene and MCE, respectively.

2.2. Source and identification of compounds

All 25 tested compounds (**1**–**25**) were isolated from the deep-sea-derived fungus *Penicillium solitum* MCCC 3A00215 [12]. The fungus was cultured on PDA plates at 28 °C for 3 d. The seed solution was cultured for 1 day, and each 1 L flask contained 400 mL of PDB culture medium. Large-scale fermentation was carried out in 48 Erlenmeyer flasks (1 L), each containing oats (80 g) and tap water (120 mL, 3% marine salt). After incubation at 25 °C for 30 days, the fermented broth was extracted with ethyl acetate three times. The filtrate was concentrated under reduced pressure to give a crude extract (200 g), which was subjected to column chromatography on a silica gel column with subsequent elution by petroleum ether, CH_2Cl_2, and ethyl acetate. The CH_2Cl_2 crude extract was separated into six fractions via medium-pressure liquid chromatography (460 mm × 36 mm) with gradient petroleum ether-ethyl acetate (5:1→1:5). Subfractions B-F were subsequently purified by column chromatography over Sephadex LH-20 (1.5 m × 3 cm; CH_2Cl_2-MeOH, 1:1) and then subjected to semi-preparative high-performance liquid chromatography with MeOH-H_2O (40%→100%) to provide 2 (280 mg). The other fractions were separated by repeated column chromatography over silica gel, ODS, Sephadex LH-20 and semipreparative high-performance liquid chromatography to afford other compounds. By comparison of the nuclear magnetic resonance (NMR) and mass spectrometry (MS) data with those published in the literature, the structures of all the compounds were determined, as shown in Fig. 1A.

Penicopeptide A (PPA, **2**) was obtained as a colorless oil and identified by comparison of NMR (Bruker 400 MHz spectrometer) and HRESIMS (Waters Q-TOF spectrometer, Xevo G2) data with literature references. HRESIMS *m/z* 583.2324 $[M + Na]^+$ (calc. for $C_{34}H_{32}N_4O_4Na$, 583.2321); ^1H NMR (400 MHz, CD_3OD) δ_H 2.62 (1 H, m), 2.74 (1 H, m), 2.86 (3 H, s), 3.02 (3 H, s), 3.19 (1 H, m), 3.36 (1 H, m), 4.33 (1 H, m), 4.40 (1 H, m), 6.96 − 7.03 (3 H, m), 7.01 (1 H, m), 7.15 − 7.22 (7 H, m), 7.28 (1 H, t, $J = 7.6$ Hz), 7.42 (1 H, t, $J = 7.4$ Hz), 7.53 (1 H, t, $J = 7.4$ Hz), 7.81 (1 H, d, $J = 7.6$ Hz), 7.96 (1 H, d, $J =$

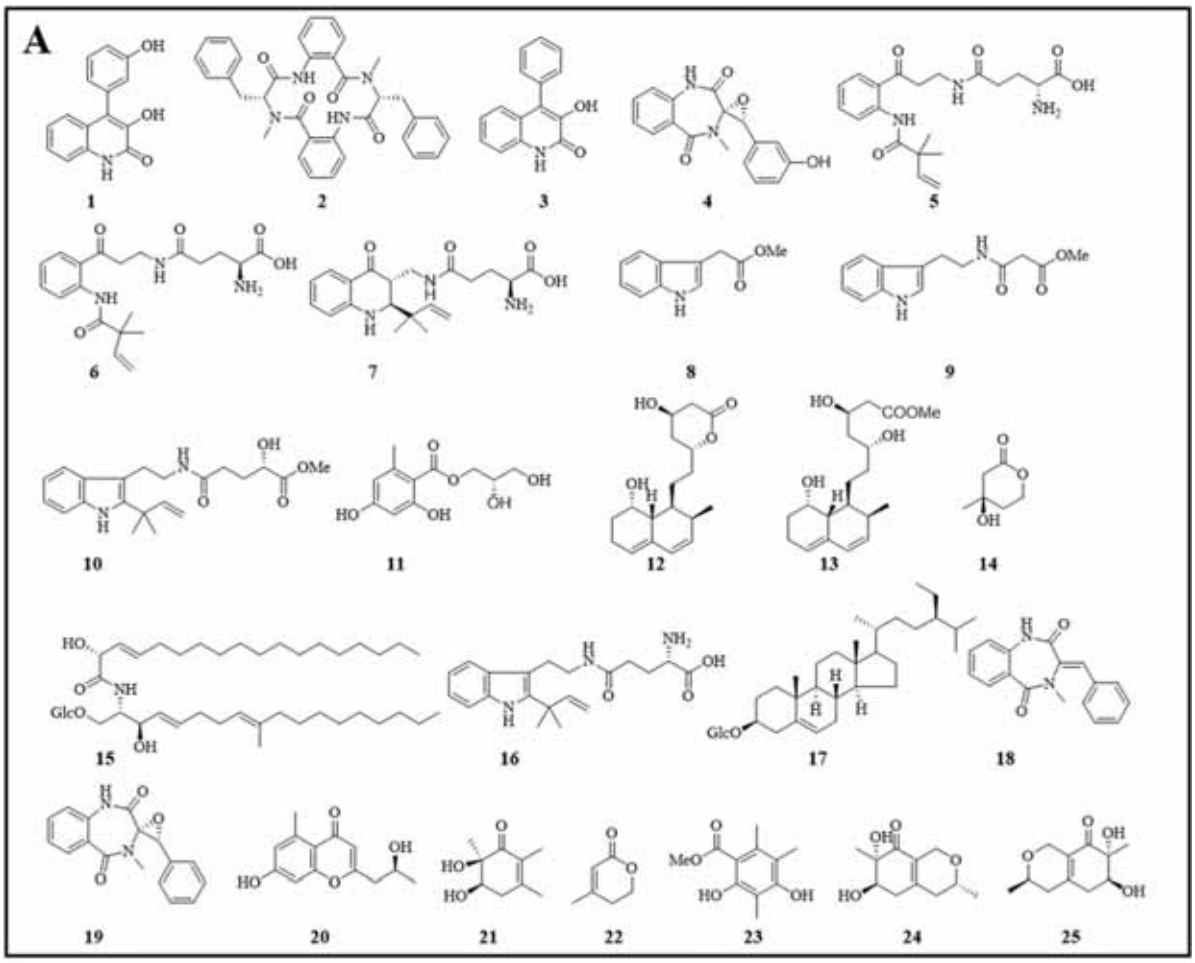

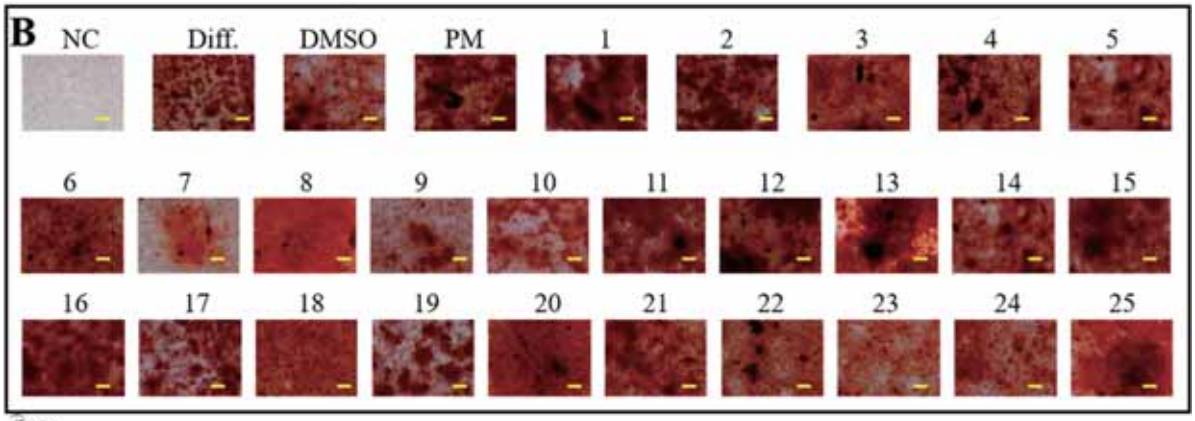

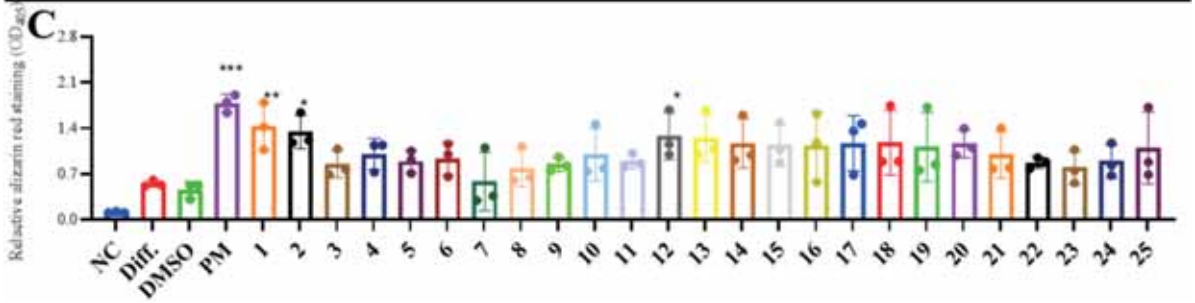

(caption on next page)

Fig. 1. Preliminary screening results for the ability of compounds from marine fungus *Penicillium solitum* MCCC 3A00215 (compounds **1**–**25**) to induce osteoblast mineralization among BMSCs. (A) Structures of compounds **1**–**25** from marine fungus *Penicillium solitum* MCCC 3A00215. (B) Alizarin Red S staining. BMSCs were exposed to compounds **1**–**25** (20 μM) and cultured for 14 days. Cells treated with the culture medium, osteogenesis differentiation medium (50 μg/mL ascorbic acid and 5 mM β-glycerophosphate), DMSO (0.1%), and purmorphamine (1 μM) were regarded as the control, differentiation, solvent, and positive control groups, respectively. Scale bar = 100 μM. (C) Quantification of Alizarin Red S staining based on optical density (OD) values. 10% acetic acid was added to every well to measure the mineralization activity among BMSCs, and absorbance was measured for quantification by a spectrophotometer (BioTek Epoch2) at 405 nm. The relative alizarin red staining was calculated as (OD_{sample}-OD_{blank})/(OD_{DMSO}-OD_{blank}). * $p < 0.05$, * * $p < 0.01$, * **$p < 0.001$ vs the DMSO group. NC, negative control; Diff, Differentiation; PM, Purmorphamine. (n = 3).

7.6 Hz); ^{13}C NMR (100 MHz, CD_3OD) δ_C 29.6, 32.8, 35.1, 39.8, 57.7, 69.4, 121.5, 121.9, 125.7, 125.8, 127.6, 127.7, 128.1, 128.2, 129.5, 129.7, 129.9, 131.8, 132.3, 133.6, 134.0, 136.8, 137.0, 137.8, 138.0, 168.0, 170.4, 171.0, 172.1.

2.3. Cell source and culture

Primary bone mesenchymal stem cells (BMSCs) and bone marrow monocytes (BMMs) were flushed from the femurs of C57BL/6J mice aged 3 weeks. Specifically, the mice were initially euthanized through cervical dislocation, and the femurs were disinfected using 75% alcohol prior to the removal of adjacent soft tissues. A sterile 1 mL syringe was employed to extract the suitable culture medium, which was subsequently introduced into the femur through the femoral head position to facilitate the release of bone marrow cells into a culture dish. This rinsing process was repeated three times. The cells were then thoroughly mixed using pipette tips and combined with an appropriate amount of complete α-MEM (containing 10% FBS and 1% penicillin/streptomycin) at a temperature of 37 °C and a CO_2 concentration of 5%.

BMMs were also isolated from the femurs of six-week-old C57BL/6J female mice. The cells were then cultured in complete α-MEM containing 30 ng/mL M-CSF at 37 °C and 5% CO_2 for 5 days to obtain BMMs.

The preosteoblast cell line MC3T3-E1 (clone 4; CRL-2593, obtained from American Type Culture Collection, Rockville, MD, USA) was a gift from Zhang Bing's laboratory. BMSCs and MC3T3-E1 cells were cultivated with complete α-MEM (Gibco) supplemented with 10% FBS (Gibco) and 1% penicillin/streptomycin (BI, Beit Haemek, Israel). Passage-2 BMSCs and passage-5 MC3T3-E1 cells were used in this experiment.

2.4. Osteogenesis mineralization assay

BMSCs were digested, plated at a density of 2×10^4 cells/well into 96-well plates and cultivated overnight. Ascorbic acid (50 μg/mL) and β-glycerophosphate (5 mM) were added to the culture medium for osteogenic differentiation, and the cells were differentiated for 14 days. Alizarin red staining was used to assess the calcification conditions in the cultures. The cells were fixed with 4% neutral-buffered formalin for 30 min and then incubated with 2% Alizarin red S for 2 min at room temperature. For quantification, 10% acetic acid was added to every well, and the absorbance was measured by a spectrophotometer (BioTek Epoch2) at 405 nm. The half-maximal effective concentration (EC_{50}) value was calculated by Prism software 9.5. Mineralization promotion (%)= (OD_{sample}-OD_{DMSO})/OD_{DMSO}× 100%.

MC3T3-E1 preosteoblasts were plated at a density of 5×10^3 cells/well into 96-well plates. After treatment with 50 μg/mL ascorbic acid and 5 mM β-glycerophosphate with or without compounds for 21 days, the cells were incubated with 2% Alizarin red S as described above for staining and quantification.

Purmorphamine is a smoothened/Smo receptor agonist with an EC_{50} of 1 μM. It was used as a positive control because it upregulates the expression of markers of osteogenic mineralization by activating the Hedgehog pathway and Smad pathway. [13–15].

2.5. Alkaline phosphatase (ALP) assay

MC3T3-E1 preosteoblasts were plated at a density of 5×10^3 cells/well into 96-well plates and treated with 50 μg/mL ascorbic acid and 5 mM β-glycerophosphate with or without compounds for 7 days. Then, the cells were incubated with 10-fold diluted alamarBlue solutions for 4 h. Then, the absorbance value was measured at 570 nm, and the cells were washed 3 times. Then, the cells were incubated with a solution containing the phosphatase substrate nitrophenol phosphate (pNPP), 6.5 mM Na_2CO_3, 18.5 mM $NaHCO_3$, and 2 mM $MgCl_2$ (Sigma—Aldrich). ALP activity was assessed using pNPP as the substrate at pH 10.2 by evaluating the optical density of the yellow substance at 405 nm. ALP activity= (OD_{sample}-OD_{blank})$_{405\ nm}$/(OD_{sample}-OD_{blank})$_{570\ nm}$× 1000.

2.6. Cytotoxicity assay

The in vitro cytotoxic bioassay was conducted using the CCK-8 method according to previously reported protocols [11]. Specifically, BMSCs were cultivated with complete α-MEM (Gibco, USA) supplemented with 10% FBS (Gibco, USA) and 1% penicillin/streptomycin. BMSCs were incubated in 96-well plates at a density of 2×10^4 cells/-well and cultured overnight. Then, the cells were treated with the test sample. After culturing for 48 h, 20 μl of CCK-8 reagent (Cellcook, CT01A, China) was added, and the cells were incubated for an additional 2 h at 37 °C. All optical densities (ODs) were measured using a microplate spectrophotometer (BioTek Epoch2) at 450 nm. The cell growth rate was calculated as follows:

Growth rate (%) = (OD_{sample}-OD_{blank})/($OD_{control}$-OD_{blank})× 100%.

MC3T3-E1 preosteoblasts were plated at a density of 5000 cells on a 96-well plates. Except for density, other operating procedures and parameters are consistent with the above.

2.7. Adipogenic differentiation

BMSCs were digested, plated at a density of 6×10^4 cells/well into 96-well plates and cultivated overnight. BMSCs were subjected to adipogenic differentiation in base differentiation medium supplemented with 0.5 μg/mL insulin, 5 μM dexamethasone, 1 μM rosiglitazone, and 0.5 mM isobutylmethylxanthine. Six days after adipogenic induction, most precursors had differentiated into mature fat cells. After washing with PBS and fixing with 4% formaldehyde, the cells were stained for 1 h at room temperature with filtered oil red O/60% isopropanol solution. Adipocytes stained red were recorded by light microscopy (Olympus CKX3-SLP, Japan) [16].

2.8. Chondrogenic differentiation

BMSCs were digested at a density of 6×10^5 cells/tube into a 15 mL centrifuge tube and centrifuged for 3 min at 1200 rpm. The supernatant was carefully discarded, 0.5 mL of medium was added to the cap of the 15 mL centrifuge tube, and the cells were cultured at 37 °C and 5% CO_2. After 24 h, the bottom of the tube was carefully and gently moved, and the cell mass was detached from the bottom of the tube and completely infiltrated into chondrogenic differentiation medium induction solution (1% insulin–transferrin–selenium solution, 10 ng/mL TGF-β3, 100 nM dexamethasone, 40 μg/mL proline, 50 μg/mL l-ascorbic acid 2-phosphate). The cells were cultured at 37 °C and 5% CO_2 for 21 days, and the freshly prepared chondrogenic differentiation induction medium was usually replaced every 2 days.

After washing with PBS twice, the cell pellet was fixed with 4%

neutral formaldehyde overnight. Then, it was directly embedded in optimal cutting temperature (OCT) compound (Sakura) and cut into 10-μm-thick sagittal sections using a cryostat (Leica). The slices were dyed with Alcian blue dye solution for 30 min. The samples were washed with tap water for 2 min and distilled water once. The effect of chondrogenic staining was observed under a microscope, and images were acquired. The effect of chondrogenic differentiation was quantified using ImageJ software.

2.9. Quantitative polymerase chain reaction (—RT-qPCR)

BMSCs were cultured with complete α-MEM containing 50 μM L-ascorbic acid and 5 mM β-glycerophosphate with or without PPA (20 μM) in 6-well plates. Total RNA was isolated with TRIzol (Vazyme, R40101AA) on day 5. One thousand nanograms of RNA was utilized to reverse-transcribe complementary DNA (cDNA) with Vazyme's HiScript II Q RT Super Mix (R22301) for —RT-qPCR. The cDNA was then used as a template for —RT-qPCR. To examine gene expression, —RT-qPCR was performed using Cham Q Universal SYBR qPCR Master Mix (Vazyme, Q71102). The $2^{-\triangle\triangle CT}$ method was used to normalize the data. The specific primers with SYBR Green (based on the mouse sequences) are listed in Table 1.

2.10. RNA sequencing (RNA-seq) and data processing

RNA-seq experiments, high-throughput sequencing and data analysis were conducted by Seqhealth Technology Co., Ltd. (Wuhan, China). Total RNA was isolated using a TRIzol kit (Promega, USA) following the manufacturer's instructions. RNA quality was determined by examining the A260/A280 ratio with a NanoDrop One spectrophotometer (Thermo Fisher Scientific Inc.). RNA integrity was confirmed by 1.5% agarose gel electrophoresis. Qualified RNAs were finally quantified with Qubit3.0 and a Qubit™ RNA Broad Range Assay Kit (Life Technologies, Q10210). After performing quality control, 1 μg total RNA samples were used for library construction. Differential expression analysis was performed with the DESeq2 Bioconductor package with a model based on the negative binomial distribution. A p value cutoff of 0.05 and fold-change cutoff of 2 were used to judge the statistical significance of differentially expressed genes (DEGs). Gene Ontology (GO) Seq (v1.34.1) was used to identify GO terms that annotated the list of enriched genes with a significant padj less than 0.05. The Kyoto Encyclopedia of Genes and Genomes (KEGG) is a collection of databases dealing with genomes, biological pathways, diseases, drugs, and chemical substances (https://www.genome.jp/kegg/). We used in-house scripts to enrich significant DEGs in KEGG pathways.

2.11. Western blotting

Western blotting was performed as previously described [17]. BMSCs were digested and plated at a density of 5×10^5 cells/well into 6-well plates. Under induction conditions (50 μg/mL ascorbic acid and 5 mM β-glycerophosphate), BMSCs were cultured with PPA (20 μM) or 0.1% DMSO (control group) for 5 days. Then, the cells were subjected to lysis utilizing RIPA buffer (Solarbic, R0010) supplemented with protease inhibitor cocktail (MCE, HY-K0010) and phosphatase inhibitor cocktail II (MCE, HY-K0022) and further centrifuged at 12,000g at 4 °C for 30 min. Equal amounts of protein (30 μg) were loaded onto a 10% SDS—PAGE gel (70 v, 25 min; 110 v, 90 min), electrophoresed and transferred to a PVDF membrane (Millipore, IPVH00010) at 250 mA for 90 min. Then, the membrane was blocked with 5% nonfat blocking grade milk and incubated with the indicated primary antibodies overnight at 4 °C. On the following day, the membranes were incubated with rabbit/mouse HRP-conjugated secondary antibodies (S0101 and S0100; 1:5000, LABLEAD, Beijing, China) at room temperature for 2 h. The immunoblots were then visualized with ultrasensitive ECL Plus chemiluminescence reagent kit (P0018S, Beyotime, Shanghai, China), and the band intensities were quantified using ImageJ software. The results were normalized using GAPDH as an internal control.

2.12. Immunofluorescence staining

BMSCs were grown on glass-bottom cell culture dishes (NEST, 801001–1, 20 mm, TC) and incubated with PPA for 5 days. The BMSCs were rinsed with ice-cold PBS twice, fixed with 4% paraformaldehyde for 30 min, and permeabilized with 0.3% Triton X-100 in PBS for 15 min. After being washed three times, the samples were blocked with 5% bovine serum albumin for 60 min and incubated with primary antibodies (mouse anti-β-catenin; 1:3000; rabbit anti-OCN; 1:200) overnight at °C. The samples were then washed, incubated with secondary antibodies (Alexa Fluor 594 anti-rabbit; 1:200 and Alexa Fluor 488 anti-mouse; 1:200) for 2 h in the dark at room temperature, and stained with DAPI (0.1 μg/mL, 1:10000) for 15 min. The cells were washed with PBS three times and viewed on a fluorescence microscope (Olympus, APEXVIEW APX100, Japan).

For immunofluorescence of bone tissue, fresh bone was collected and immediately fixed in ice-cold 4% paraformaldehyde solution overnight. The samples were decalcified by daily changes of 0.5 M EDTA for 6 weeks at 4 °C with constant shaking. All samples were embedded in OCT compound (Sakura) and cut into 40-μm-thick sagittal sections using a cryostat (Leica). Immunofluorescence staining and analysis were performed as described previously. [17] Briefly, sections were treated with 0.3% Triton X-100 for 15 min. Then, the sections were blocked with 5% donkey serum at room temperature for 30 min and incubated overnight at 4 °C with antibodies against β-catenin (1:3000 dilution) and GSK-3β (1:800 dilution), which were visualized with species-appropriate Alexa Fluor-coupled secondary antibodies. The nuclei were counterstained with DAPI for 30 min. An Olympus APX100 confocal microscope or Leica confocal microscope (Leica, TCS SP8 DLS, Germany) was used to image samples. The fluorescence quantitation was calculated using ImageJ software.

2.13. Molecular docking

The structure of the protein (GSK-3β: 5OY4; AKT: 4RDJ) was downloaded from the Protein Data Bank (PDB). We used ligand docking in the Glide module of Schrödinger software (Schrödinger Maestro, New York, NY, USA, Version 11.1.011, MM Version 3.7.011, Release 2017–1, Platform Windows-x64) to study the docking. First, the grid file was generated by receptor generation. Ligands were prepared using the force field OPLS3e, and possible states were generated from pH 7.0 + /- 2.0. The protein was prepared by restrained minimization using the OPLS3e force field. The grid sites were created using a Glide® receptor grid

Table 1
Sequences of the primers used in —RT-qPCR.

Genes	Forward (5'->3')	Reverse (5'->3')
Runx2	CCTGAACTCTGCACCAAGTCCT	TCATCTGGCTCAGATAGGAGGG
Ibsp	AATGGAGACGGCGATAGTTCCG	GGAAAGTGTGGAGTTCTCTGCC
Bglap	GCCAATGGCAAAGATGACCACAG	TGCGTGGAGTATCCATCTCTGC
HIVEP3	CTGGTTCCATCCAACTCCCGAA	CCTCTCTTGGAAGTGGGAGTAC
HPRT	CTGGTGAAAAGGACCTCTCGAAG	CCAGTTTCACTAATGACACAAACG

generator with a docking length of 20 Å. The center of the grid box was consistent with the center of the ligand in the crystal file (PDB). The remaining parameters were the default parameters. Glide uses standard precision SP for semiflexible docking. The Epik module was used to penalize the docking scoring function, and the default parameters were used for other docking parameters. Molecular docking was carried out with ligand docking in the Schrodinger Glide module. The above grid file and the prepared small molecule compounds were selected, and the docking program was run according to the set parameters. The docking scores are reported as kcal/mol; the more negative the number is, the better the binding. The final docking results were drawn and exported by PyMOL.

2.14. Surface plasmon resonance (SPR) assay

Chemically modified label-free photocrosslinker sensor chips were provided by Betterways Inc. (China). For array spotting, a BioDot™ AD-1520 Array Printer (BIODOT Inc., USA) was employed to print samples and controls on the surface. Each candidate compound was printed with a volume of 1.875 nl/dot using the BioDot 1520 array printer to form four nonadjacent replicates of each sample on the same chip. Then, the flow cell chambers were assembled onto the chip surface, and the chips were inserted and tested in the SPR instrument one after another. To validate the ability to detect chemical compound-protein interactions using the photocrosslinker SPR sensor chip, we selected rapamycin and biotin as system controls and arranged kinetic constant tests with FKBP12 on rapamycin and biotin with streptavidin immediately after the sample tests. Additionally, the solvents for chemical compounds (DMSO) and for proteins (PBS, pH=7.0) were crosswise tested individually as blank controls and background noise controls. To monitor the enrichment process of the target protein, we performed a real-time SPR experiment using a bScreen LB 991 Label-free Microarray System (Berthold Technologies, Germany). During the SPR test, the chip surface was first primed three times with HBS-EP running buffer (containing 10 mM HEPES, pH 7.0, 150 mM NaCl, 3 mM EDTA and 0.005% (v/v) P20 surfactant) at a rate of 2 μl/s for 40 s and one time with running buffer (1 × PBS with 5% DMSO) at a rate of 2 μl/s for 40 s. The mouse AKT protein (Origene, TP507696, USA, Maryland) and GSK-3β protein (MCE, HY-P73090, USA, New Jersey) were diluted separately with running buffer at concentrations of 10 nM, 40 nM, 160 nM, 640 nM, and 2560 nM and injected over 600 s at a flow rate of 0.5 μl/s in each associating stage, after which running buffer was injected for 360 s at a flow rate of 0.5 μl/s in each dissociating stage. At the end of each association–dissociation cycle, the surface was regenerated to remove any remaining bound material with a pulse of 10 mM glycine-HCl (pH 2.5) at 2 μl/min for 300 s

2.15. Ovariectomy (OVX)-induced osteoporosis mouse model

We established an OVX-*induced osteoporosis mouse model* according to a previously described standard protocol [19]. C57BL/6 J mice (n = 24, approximately 20 g, female, 10 weeks, Gempharmatech Co., Ltd) were used to establish an OVX mouse model and then randomly segmented into three groups (n = 8): the sham (without surgery), OVX + vehicle and OVX + 10 mg/kg PPA groups. Bilateral OVX was carried out to induce systemic osteoporosis based on previously described procedures after the mice were anesthetized with isoflurane. The mice in the sham or OVX group were administered a tail vein injection of normal saline, and the mice in the OVX+PPA group were injected with 10 mg/kg PPA every second day. All mice were sacrificed at the 6th week. Calcein (20 mg/kg) was given to all the mice s.c. at − 8 and − 1 days before euthanasia.

2.16. Micro-computed tomography (μCT) and bone histomorphometry analysis

The right femurs were fixed with 4% paraformaldehyde overnight and then placed in 75% ethanol. The distal femurs and middle femurs were scanned with high-resolution μCT (SkyScan1272, United States) as described [17]. Images from the μCT scans were reconstructed by the NRecon program. Then, the reconstructed images were analyzed by the cTAn program. Bone volume/tissue volume (BV/TV), trabecular thickness (Tb.Th), trabecular separation (Tb.Sp), trabecular number (Tb.N), and cross-sectional thickness (Cs.th) or cortical bone volume are reported.

The femurs after μCT scanning and lumbar vertebrae were further decalcified in 10% EDTA at room temperature for 6 weeks. Then, they were embedded in resin for bone histomorphometric analysis. Seven-micrometer sections were taken for toluidine blue staining, Von Kossa staining, and double fluorescence labeling of calcium. Sections of 5 μm were used for TRAP staining. The quantitative parameters, including osteoblast surface/bone surface (Ob.S/BS), osteoclast number/bone surface (N.Oc./B.Pm), mineralizing surface/bone surface (MS/BS), mineral apposition rate (MAR), and bone formation rate/bone surface (BFR/BS) were analyzed with OsteoMeasure software (OsteoMetrics, USA).

2.17. Statistical analysis

All experiments in this research were independently repeated at least three times. The data are expressed as the mean ± standard deviation (SD). GraphPad Prism 8.0 was used to perform statistical analyses. Student's t test was used to compare two groups, and Dunnett's test (in which each group was compared with the control group) or Tukey's test (in which each group was compared with other groups) was used to perform one-way ANOVA for multiple comparisons. The results with $^{*}p < 0.05$, $^{**}p < 0.01$, $^{***}p < 0.001$, and $^{****}p < 0.0001$ were regarded as statistically significant.

3. Results

3.1. Screening of compounds for the ability to induce osteogenic mineralization

All 25 compounds (**1**–**25**) from marine fungus *Penicillium solitum* MCCC 3A00215 were evaluated for their effect of osteogenic mineralization by BMSCs. At a concentration of 20 μM, compounds **1**, **2**, and **12** showed an obvious promoting effect on osteogenic mineralization among BMSCs, as evidenced by the significant increases in mineralized nodules induced by these three compounds. Compared with the control group, the quantitative osteogenic effect reached more than 1.5-fold (Fig. 1). Thus, these three active compounds (**1**, **2**, and **12**) were selected to further determine the corresponding EC_{50} values for mineralization. The EC_{50} values for compounds **1**, **2**, and **12** were 4.408, 20.310, and 21.43 μM, respectively (Fig. 2S, supplementary information). The high yield of PPA (**2**, 280 mg) indicates its potential for development and application as a candidate drug. Considering the quantity, the novelty of its structure and its uncharacterized effect on bone metabolism, we ultimately selected PPA for further investigation of its anti-osteoporosis activity and the underlying mechanism. The two-dimensional and three-dimensional structures of PPA are presented in Fig. 2A-B.

3.2. PPA stimulates osteogenic mineralization among BMSCs without cytotoxicity

BMSCs are able to differentiate into osteoblasts, chondroblasts, and adipocytes, [18] and bone regeneration achieved via osteogenic induction of MSCs could provide a rational therapeutic strategy for preventing

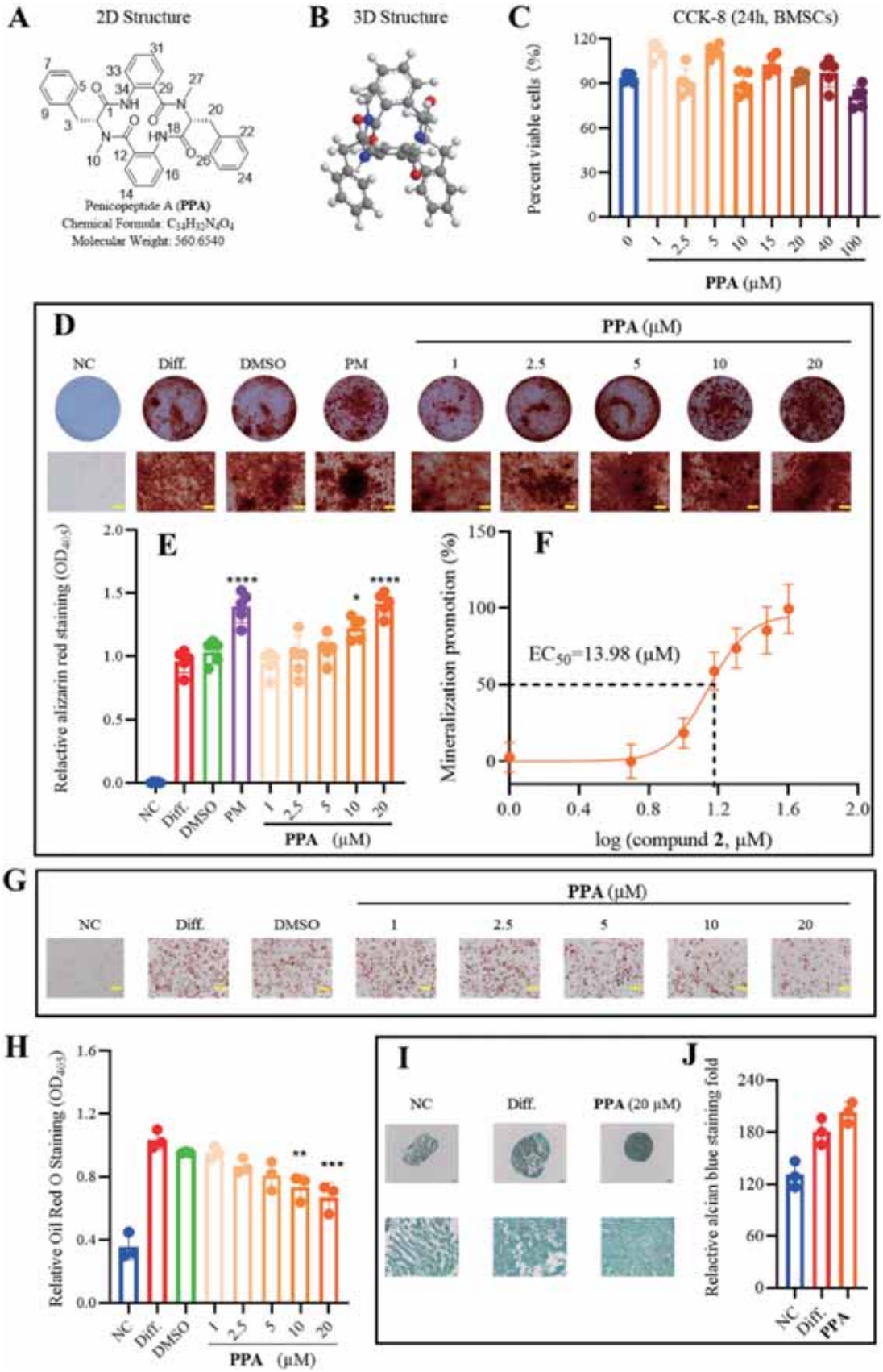

(caption on next page)

Fig. 2. PPA stimulates osteoblastic mineralization and inhibits adipogenic differentiation among BMSCs. (A, B) 2D and 3D chemical structures of PPA. (C) BMSC viability upon treatment with PPA as measured by the CCK-8 assay. BMSCs were cultured with PPA (0 μM to 100 μM) for 48 h. All PPA used for testing was dissolved in dimethyl sulfoxide (DMSO) as stock solution and further diluted in culture medium for use in assays. DMSO was the solvent control, with a working concentration of 0.1%. (n = 5) (D) Alizarin Red S staining. Under the induction conditions (50 μg/mL ascorbic acid and 5 mM β-glycerophosphate), BMSCs were exposed to PPA (1, 2.5, 5, 10, or 20 μM) for 14 days. Normal culture medium, osteogenesis differentiation medium, 0.1% DMSO, and purmorphamine (1 μM) were regarded as the negative control (NC), differentiation (Diff.), solvent, and positive control groups, respectively. Scale bar = 100 μM. (n = 5) (E-F) Quantification of Alizarin Red S staining and EC_{50} value calculation. (G) Oil red O staining. Under the induction conditions (0.5 μg/mL insulin, 5 μM dexamethasone, 1 μM rosiglitazone, and 0.5 mM isobutylmethylxanthine), BMSCs were treated with PPA (1, 2.5, 5, 10, or 20 μM) for 6 days. Normal culture medium, adipogenic differentiation medium, and 0.1% DMSO were regarded as control, differentiation, and solvent groups, respectively. Scale bar = 100 μM. (n = 3) (H) Quantification of Oil red O staining with isopropanol. (n = 3) (I) Alcian Blue staining. Under the induction conditions (1% insulin transferrin-selenium solution, 10 ng/mL TGF-β3, 100 nM dexamethasone, 40 μg/mL proline, and 50 μg/mL L-ascorbic acid 2-phosphate), BMSCs were exposed to PPA (20 μM) for 21 days. Normal culture medium, chondrogenic differentiation medium, and 0.1% DMSO were regarded as control, differentiation, and solvent groups, respectively. Scale bar = 100 μM and 20 μM (J) Quantification of Alcian Blue staining with ImageJ. (n = 3) * $p < 0.05$, * * $p < 0.01$, * ** $p < 0.001$, * ** * $p < 0.0001$ vs the DMSO group. NC, negative control; Diff, Differentiation; PM, Purmorphamine.

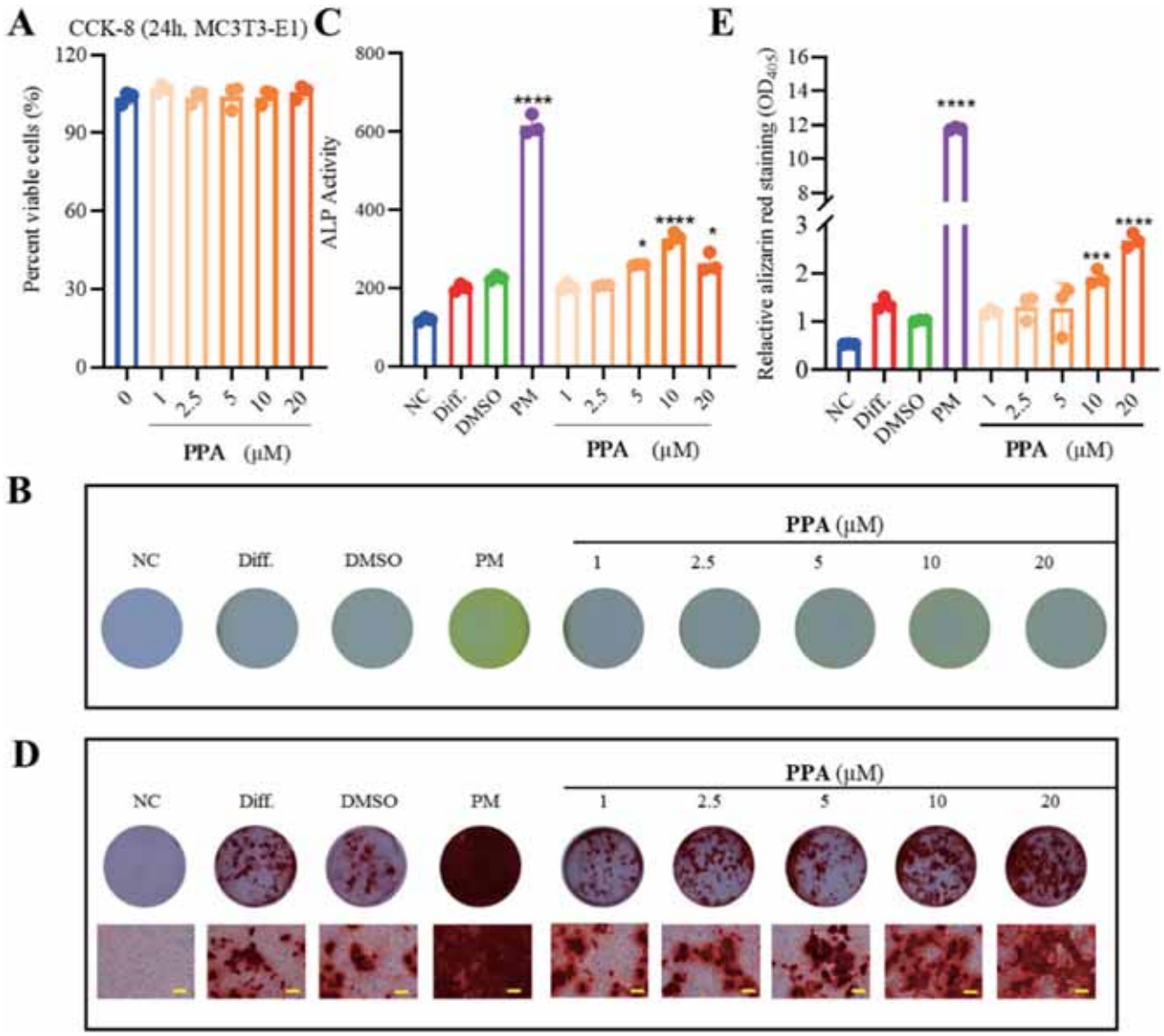

Fig. 3. PPA promotes osteogenic differentiation and mineralization among MC3T3-E1 cells. (A) The cytotoxicity of PPA was assessed using the CCK-8 assay. The MC3T3-E1 cells were treated with PPA (1, 2.5, 5, 10, or 20 μM) for 48 h. (B) ALP activity of MC3T3-E1 cells treated with different concentrations of PPA. Under the induction conditions (50 μg/mL ascorbic acid and 5 mM β-glycerophosphate), MC3T3-E1 cells were cultured with PPA (1, 2.5, 5, 10, or 20 μM) for 7 days. Normal culture medium, adipogenic differentiation medium, and 0.1% DMSO were regarded as control, differentiation, and solvent groups, respectively. (C) Quantification of ALP activity. (D) Alizarin Red S staining. Under the induction conditions (50 μg/mL ascorbic acid and 5 mM β-glycerophosphate), BMSCs were treated with PPA (1, 2.5, 5, 10, or 20 μM) for 6 days. Normal culture medium, osteogenesis differentiation medium, 0.1% DMSO, and purmorphamine (1 μM) were regarded as the negative control (NC), differentiation (Diff.), solvent, and positive control groups, respectively. Scale bar = 100 μM (E) Quantification of Alizarin Red S staining. * $p < 0.05$, * * $p < 0.01$, * ** $p < 0.001$, * ** * $p < 0.0001$ vs the DMSO group. NC, negative control; Diff, Differentiation; PM, Purmorphamine. (n = 3).

age-related osteoporosis [7]. Therefore, we investigated the ability of PPA to directly induce BMSC differentiation into osteoblasts. First, we assessed the potential toxicity of PPA to BMSCs. As shown in Fig. 2C, PPA at concentrations ranging from 0 μM to 100 μM had no cytotoxic effect on BMSCs. Then to determine the effective concentration of PPA for stimulating OB differentiation among BMSCs, BMSCs were treated with different concentrations of PPA (1, 2.5, 5, 10, 20, 30 and 40 μM) and osteoblast formation was evaluated based on osteogenic mineralization among the cells. As shown in Fig. 2D-F, PPA significantly promoted the mineralization of BMSCs in a concentration-dependent manner.

3.3. PPA suppresses adipogenic differentiation of BMSCs with no apparent effect on the chondrogenic differentiation of BMSCs

The adipogenic differentiation of BMSCs was detected by staining with oil red O. As shown in Fig. 2G-H, after treatment with PPA (10 or 20 μM), the percentage of adipogenic cells was decreased significantly. This result indicated that PPA suppresses the adipogenic differentiation of BMSCs in a dose-dependent manner. Additionally, the chondrogenic differentiation of BMSCs exposed to the same concentrations of PPA was assessed by Alcian Blue staining. Treatment with chondrogenic induction medium resulted in a change in cell morphology from a spindle shape to an ellipsoidal and triangular shape, and the staining results showed that PPA did not influence the chondrogenic differentiation of BMSCs (Fig. 2I-J).

3.4. PPA promotes osteogenic differentiation and mineralization among MC3T3-E1 cells

To further validate the osteogenic activity of the PPA, we also assessed the effect of PPA on the osteogenic differentiation of the MC3T3-E1 osteoblastic cell line by measuring the ALP activity and mineralization activity of cells after treatment with PPA. We first confirmed that PPA did not reduce the viability of MC3T3-E1 cells (Fig. 3A). As shown in Fig. 3B-C, PPA promoted ALP activity, with a lowest effective concentration of 5 μM. As shown in Fig. 3D-E, matrix mineralization in MC3T3-E1 cells was enhanced by treatment with PPA at concentration of 10 and 20 μM. Compared with the solvent group, the highest tested concentration of PPA (20 μM) resulted in a 3-fold greater amount of osteoblastic mineralization. Combined with the experiments presented above, these results confirmed the osteogenic effects of PPA on BMSCs and MC3T3-E1 cells.

3.5. PPA induces osteogenesis via PI3K-AKT signaling

The mechanism of the osteogenic induction ability of PPA in BMSCs was explored by RNA-sequencing (RNA-seq). Principal component analysis (PCA) as correlation analysis demonstrated that the control and PPA-treated groups had good intra-group consistency and differences (Fig. 4A). Volcano plot analysis revealed that 1540 genes were upregulated by more than 2-fold, while another 1399 genes were considerably downregulated in PPA-treated cells compared with control cells. Heat map analysis and volcano plot analysis consistently showed the differential expression of a wide range of genes between the two groups (Fig. 4B-C). GO enrichment analysis of the differentially expressed genes identified 1281 biological processes ($p < 0.05$), including processes involved in the regulation of ossification, bone mineralization, bone morphogenesis, biomineralization, and osteoblast differentiation (Fig. 4D). KEGG analysis showed that the differentially expressed genes were associated with functional annotation changes realized through the PI3K-AKT, MAPK, calcium, tumor necrosis factor (TNF), and transforming growth factor beta (TGF-β) signaling pathways. Of these, the PI3K-AKT, MAPK, and calcium signaling pathways are well known to be involved in osteoblast formation. From this short list, the PI3K-AKT signaling pathway was considered the most likely mechanism of PPA-induced osteogenesis based on its best enrichment and the corresponding p value (Fig. 4E).

3.6. PPA stimulates expression of osteoblast-specific genes and proteins by activating the AKT/GSK-3β/β-catenin signaling pathway

To further elucidate the signaling mechanisms by which PPA promotes osteogenic activity, we explored the involvement of the AKT/GSK-3β/β-catenin signaling pathway. The expression levels of AKT, phosphorylated (p)-AKT, GSK-3β, p-GSK-3β, and β-catenin in PPA-treated BMSCs were examined by western blot analysis. p-AKT and p-GSK-3β expression levels were promoted by treatment with PPA for 5 days, whereas the total AKT and GSK-3β expression levels remained unchanged by PPA treatment. The expression level of β-catenin was significantly increased by PPA (Fig. 5A-C). p-AKT can prevent GSK-3β from forming a complex with β-catenin, resulting in the accumulation of β-catenin. Furthermore, p-GSK-3β is known to exacerbate this phenomenon [19,20].

To verify whether the AKT/GSK-3β/β-catenin signaling pathway is activated by PPA treatment in BMSCs, we performed immunofluorescence staining to detect the level of β-catenin and its co-location with osteocalcin (OCN) in BMSCs. Immunofluorescence results showed that the OCN levels and nuclear translocation of β-catenin were significantly increased in BMSCs cells treated by PPA, compared with the control group (Fig. 6A). Thus, PPA may promote osteogenic gene expression of *Runx2*, *Ibsp,* and *Bglap* and inhibit expression of the negative osteogenic gene *HIVEP3* (Fig. 5D) to enhance osteogenic differentiation and mineralization among BMSCs. Moreover, we have assessed β-catenin and GSK-3β activity via immunofluorescence staining in OVX mice. The results also demonstrated that PPA does indeed promote the expression of β-catenin in vivo but had no significant effect on GSK-3β protein expression. This is consistent with the mechanistic results in vitro. (Fig. 6B).

3.7. PPA interacts with AKT and GSK-3β

To identify the possible targets of PPA on the two potential interacting proteins AKT (PDB: 4DRJ) and GSK-3β (PDB: 5OY4) as well as the possible interaction modes, the Schrodinger was used for molecular docking analysis. Amino acid residues within distance of 5 Å around the docked ligand were labeled. As indicated in Fig. 7A-B, PPA could smoothly enter the active binding pocket of 4DRJ. A microcosmic site in 4DRJ indicated that the high affinity between PPA and 4DRJ is based on their complex interactions of H-bonding and Pi-Pi-stacking. The vital residues included TYR113, SER118, and LYS121. Moreover, 4DRJ had a stronger affinity for PPA (docking score = −5.500) than its native ligand (native ligand docking score = −4.109; Fig. 7C-D). We also found that PPA bound to the key targets' active pocket in protein 5OY4 through Pi-cation bonding connections with LYS183 (Fig. 7E-F). The PPA and 5OY4 were considered to have good binding activity with a docking score of − 5.507 kcal/mol (Fig. 7G-H).

Surface plasmon resonance (SPR) technology has been widely used to monitor the kinetics of ligand/protein interactions. To further verify the binding mode and ability, the binding affinity of PPA towards AKT and GSK-3β was evaluated using a SPR assay. The results revealed a concentration-dependent SPR signal, indicating direct interaction. PPA exhibited a strong binding affinity towards AKT, characterized by a fast association and fast dissociation mode, with a K_D value of 214 nM. Similarly, PPA displayed a fast association and fast dissociation towards GSK-3β, with a K_D value of 177 nM (Fig. 7I). Together, these data illustrate that PPA closely interacts with key targets on AKT and GSK-3β.

3.8. PPA ameliorates OVX-induced bone loss

An OVX model was used to validate the therapeutic value of PPA in inhibiting osteoporosis in *vivo*. OVX mice received injections of 10 mg/

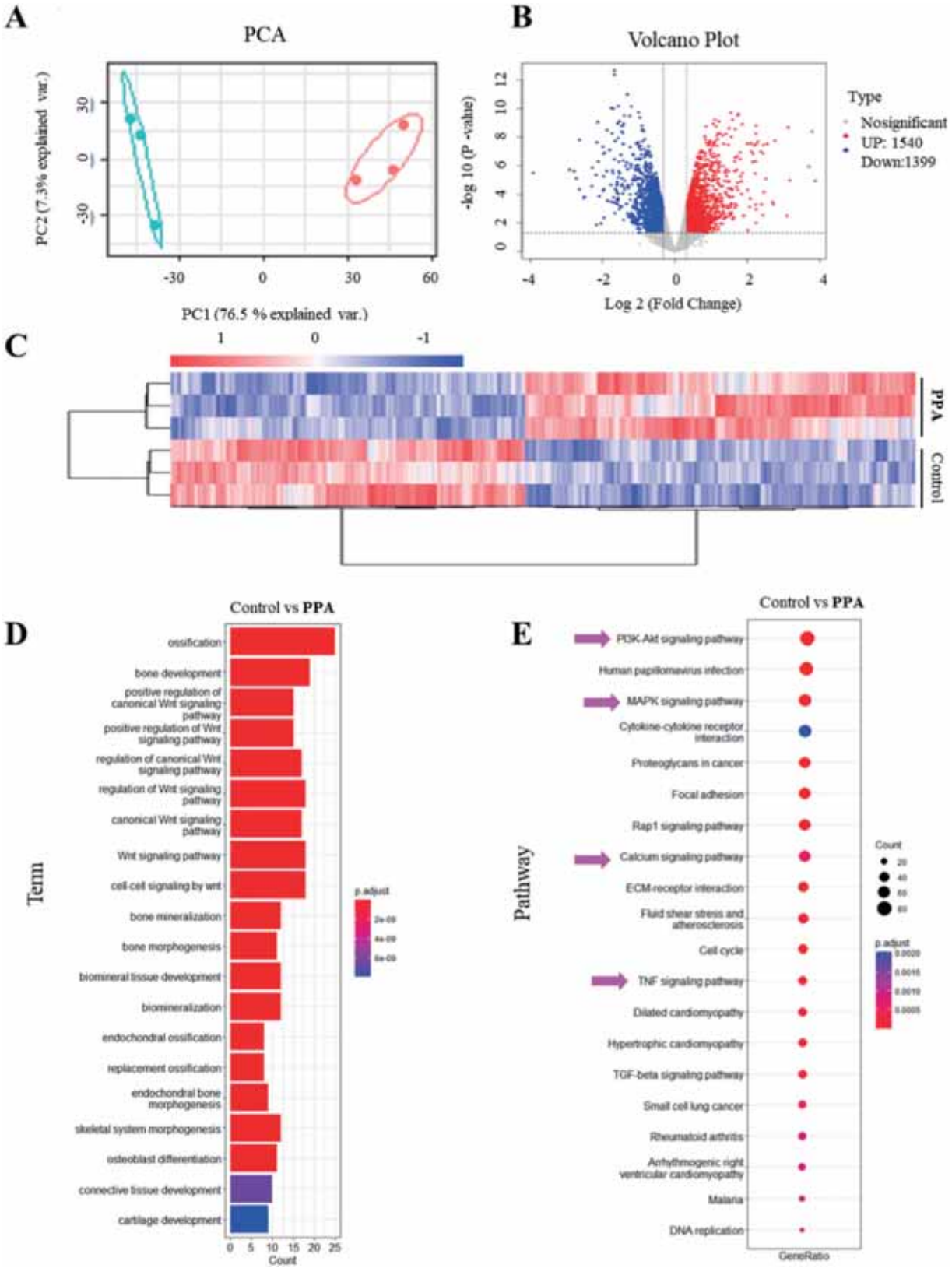

Fig. 4. RNA-sequencing to explore the mechanism of PPA-induced osteogenesis in BMSCs. Under the induction conditions (50 μg/mL ascorbic acid and 5 mM β-glycerophosphate), BMSCs were exposed to PPA (20 μM) for 5 days. 0.1% DMSO was the control treatment. (A) PCA of genes expression between different samples. (B) Volcano plot of the differentially expressed genes in the control vs PPA groups. The log2-fold change and p-value are shown for some osteoblastogenesis-related genes. (C) Heatmap analysis of the differentially expressed genes in the PPA-treated group compared with the control group. (D) GO analysis of some differentially expressed genes. (E) KEGG analysis of all differentially expressed genes.

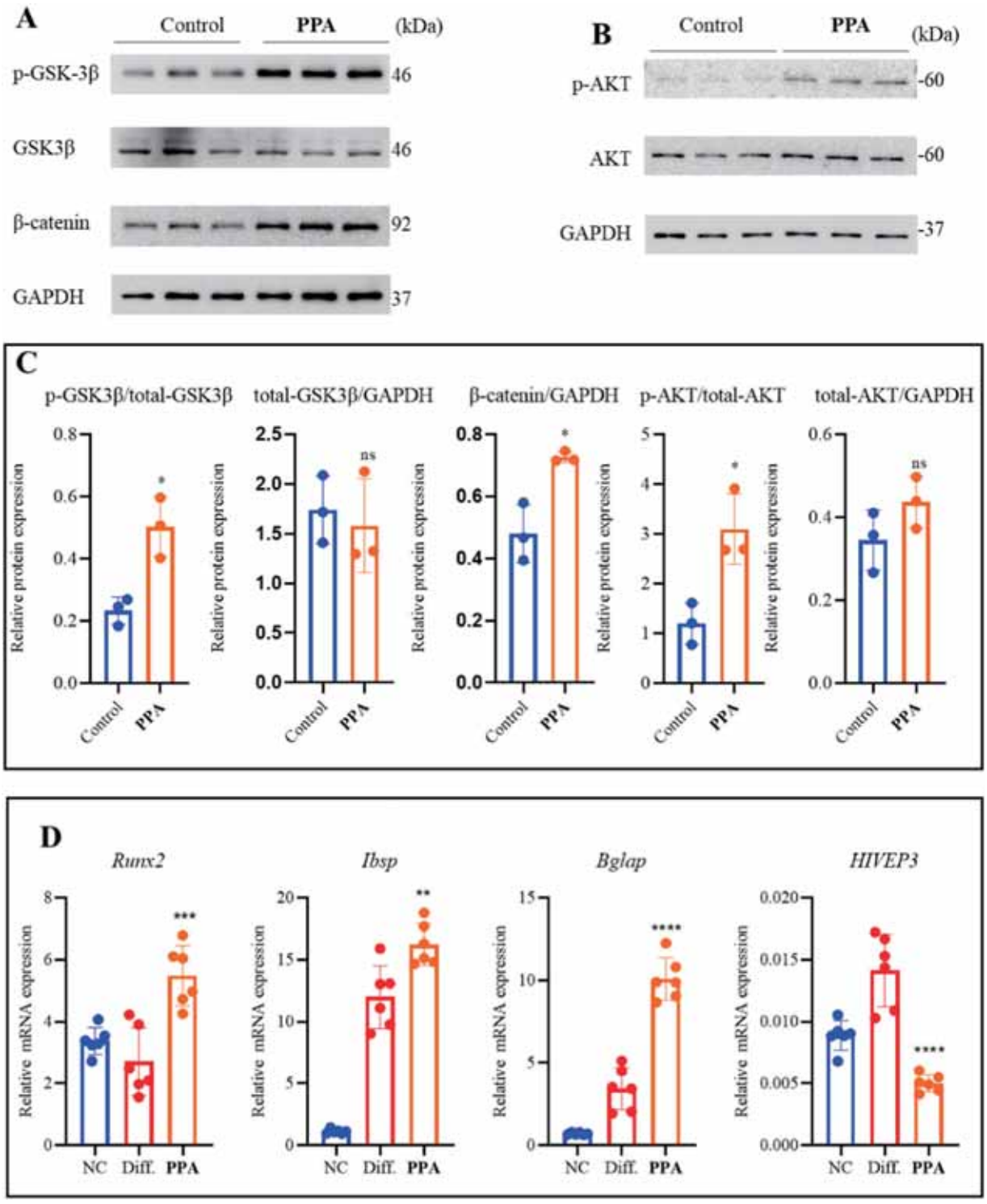

Fig. 5. PPA stimulates expression of osteoblast-specific genes and proteins. Under the induction conditions (50 μg/mL ascorbic acid and 5 mM β-glycerophosphate), BMSCs were treated with PPA (20 μM) for 5 days. (A) Representative images of western blots reflecting the expression levels of GSK-3β, phosphorylated (p)-GSK-3β, and β-catenin normalized to GAPDH (n = 3). (B) Representative images of western blots reflecting the expression levels of AKT and p-AKT normalized to GAPDH (n = 3). (C) Quantitative analysis of the fold change in AKT, p-AKT, GSK-3β, p-GSK-3β, and β-catenin expression. Gene expression levels relative to Hprt expression in BMSCs after 5 days of PPA treatment. (D) PPA induced expression of osteogenic specific genes: *Runx2*, *Ibsp*, *Bglap*, and *HIVEP3*. NC, negative control; Diff, Differentiation. * $p < 0.05$, * * $p < 0.01$, * ** * $p < 0.001$, * ** * * $p < 0.0001$ vs the DMSO group. (n = 6).

kg PPA (OVX+PPA group) or 0.25% DMSO-NS (OVX + Vehicle group) via the caudal vein every 2 days for 6 weeks before being euthanized. We found that injections of PPA for 6 weeks did not change body weights or cause any visible side effects (Supplementary Fig. 1 S).

Micro-computed tomography (CT) showed that PPA treatment prevented bone loss caused by OVX in mouse femurs (Fig. 8A). Quantitatively, as indicated in Fig. 8B–E, compared with the sham group, the OVX + Vehicle group showed decreases in the bone volume to total volume ratio (BV/TV), trabecular number (Tb.N), and trabecular thickness (Tb.Th) by approximately 32.6%, 37.2%, and 6.1%,

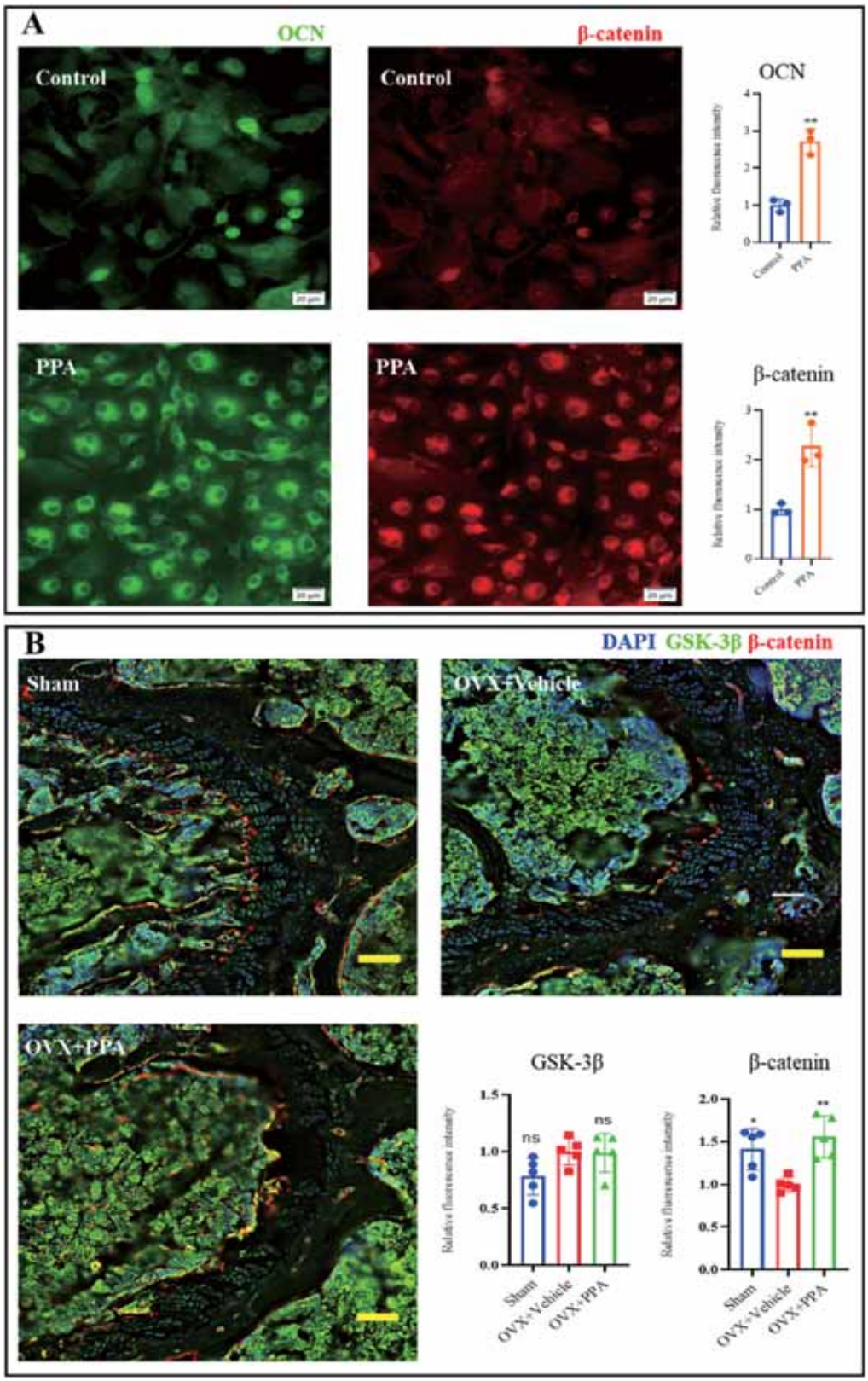

Fig. 6. PPA promoted expression of OCN and β-catenin. (A) Representative images and quantification of immunofluorescence staining of OCN and β-catenin treated with 20 μM PPA for 5 days. All the BMSCs from control and PPA group were cultured for osteogenic differentiation (50 μg/mL ascorbic acid and 5 mM β-glycerophosphate). The final DMSO concentration in cells treated with different concentrations of PPA was also 0.1%. The control group also contain 0.1% DMSO. Scale bar = 20 μm. (n = 3) * * $p < 0.01$ vs the control group. (B) Representative images of femur sections from sham mice, OVX mice, and OVX mice treated with 10 mg/kg PPA, and quantification of immunofluorescence staining of GSK-3β and β-catenin in vivo. The femur was used for bone histomorphometric analysis. After being fixed in 4% paraformal dehyde, decalcified with 0.5 M EDTA at 37 °C for 6 weeks, paraffinembedded and sectioned, 40-μm femur sections were stained for GSK-3β (green) and β-catenin (red) with DAPI nuclear staining (blue). Scale bars, 50 μm. (n = 5) * $p < 0.05$, * * $p < 0.01$ vs the OVX+Vehicle group.

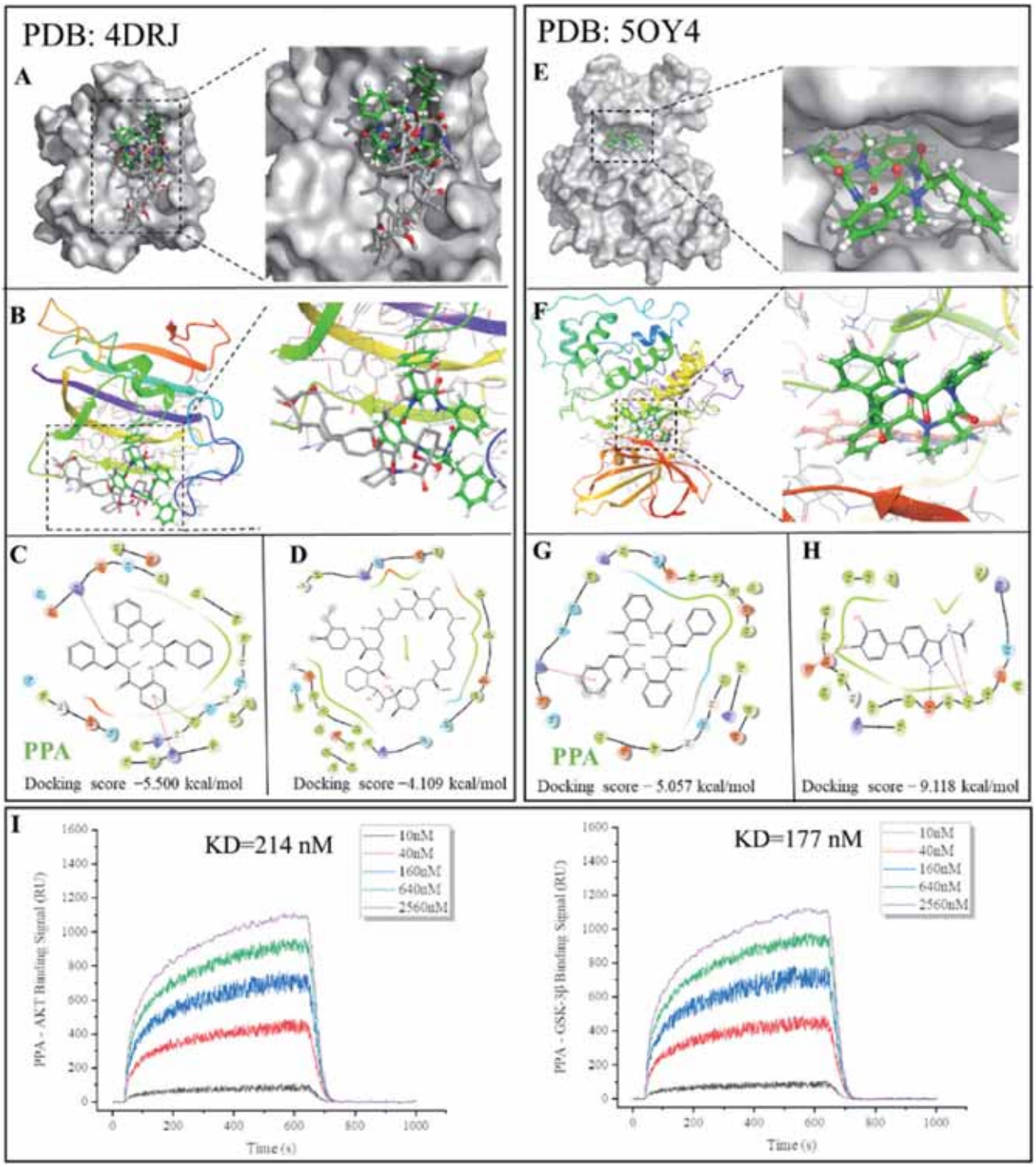

Fig. 7. Molecular docking of PPA toward AKT (4DRJ) and GSK-3β (5OY4). An absolute docking score of > 4.25 but < 5 represents potential binding activity; ≥ 5 but < 7, good binding activity; and ≥ 7, strong binding activity. In the 3D structural analysis, the ligand of 4DRJ (grey), ligand of 5OY4 (faded red-orange), and PPA (green) are presented in a colored stick model. The nitrogen/oxygen atoms in the structure appear red/dark blue. (A). Comparison of binding modes of PPA and native ligand of 4DRJ in a 3D workspace surface. (B) Comparison of binding modes of PPA and native ligand of 4DRJ in a 3D workspace cartoon. (C) 2D combination mode diagram of PPA with 4DRJ. The H-bonding and Pi-Pi-stacking are presented as a purple arrow and green thread, respectively. (D) 2D combination mode diagram of native ligand with 4DRJ. (E) Comparison of binding modes of PPA and native ligand of 5OY4 in a 3D workspace surface. (F) Comparison of binding modes of PPA and native ligand of 5OY4 in a 2D cartoon. (G) 2D combination mode diagram of PPA to 5OY4. The Pi-cation bonding is presented as a red thread. (H) 2D combination mode diagram of ligand to 5OY4. The H-bonding is presented as a purple arrow. (I) SPR results for PPA binding to AKT and GSK-3β.

respectively, along with a 15.6% increase in the trabecular separation (Tb/Sp). These data confirm that bone loss was serious after OVX model generation, and thus, the experimental model data for bone loss are reliable. Compared with OVX + Vehicle only, treatment with PPA after OVX resulted in increases in BV/TV and Tb.N. (Fig. 8B) Consistent with the micro-CT analysis results, Von Kossa staining also indicated that PPA treatment lessened bone loss after OVX. Furthermore, Toluidine blue staining and tartrate-resistant acid phosphatase (TRAP) staining of

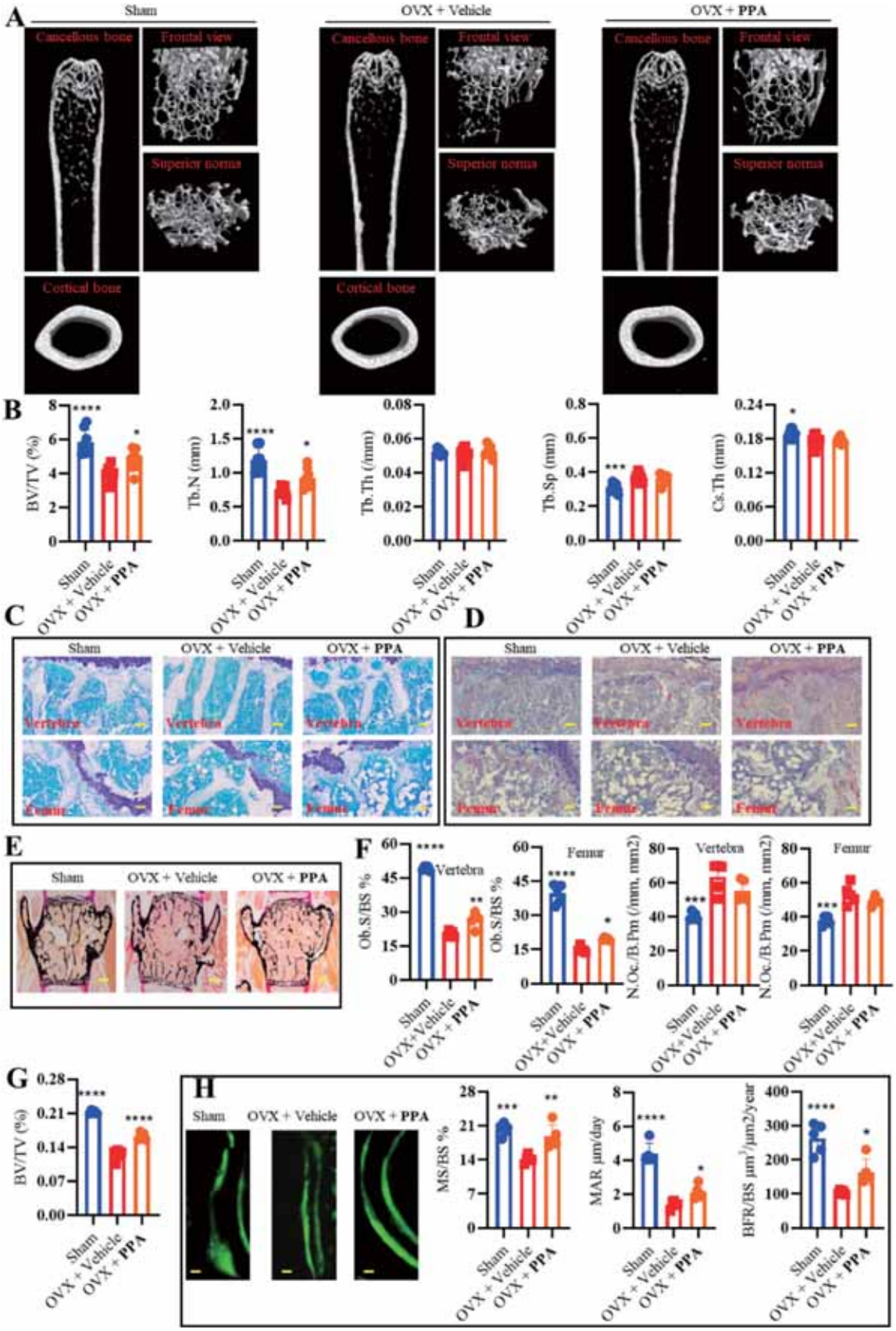

(caption on next page)

Fig. 8. PPA ameliorates OVX-induced bone loss in vivo. (A) 3D reconstructions of images from micro-CT scans of femurs from the sham, vehicle, and PPA (10 mg/kg) groups (n = 8). (B) Quantitative measurements of bone microstructure-related parameters: BV/TV, Tb.Sp, Tb.N, Tb.Th, and Cs.Th. (C-E) Representative images of decalcified bone stained with Toluidine blue (C), TRAP (D), and Von Kossa (E) from each group. Scale bar = 100 μM for C and D, 250 μM for E. (F–G) Quantitative measurements of static bone remodeling: Ob.S/BS, N.Oc./B.Pm and BV/TV. (H) Representative fluorescence images of double calcein-labeled sections of vertebra and quantitative measurements of dynamic bone remodeling: MS/BS, MAR, and BFR/BS. * $p < 0.05$, * * $p < 0.01$, * ** $p < 0.001$, * ** * $p < 0.0001$ vs the OVX + Vehicle group. BV/TV, bone volume/total volume; Tb.Sp, trabecular separation; Tb.N, trabecular number; Tb.Th, trabecular thickness; Cs.Th, cortical width; Ob.S/BS, osteoblast surface per bone surface; N.Oc./B.Pm, osteoclast number/bone surface; MS/BS mineralizing surface/bone surface; MAR, mineral apposition rate; BFR/BS, bone formation rate/bone surface.

histological sections of femurs and vertebrae showed that OVX + Vehicle dramatically decreased the osteoblast surface per bone surface ratio (Ob.S/BS) and increased the osteoclast number per bone surface ratio (N.Oc.S/B.Pm), whereas PPA treatment notably rescued this change (Fig. 8C-G). Dynamic bone remodeling was monitored by fluorescence double labeling, which showed that three parameters corresponding to osteoblast activity increased with PPA treatment. Specifically the mineralizing surface to bone surface ratio (MS/BS), the mineral apposition rate (MAR), and the bone formation rate to bone surface ratio (BFR/BS) were 24.8%, 34.1%, and 36.1% greater in the PPA treated group than in the OVX + Vehicle only group, respectively, indicating an overall increase in bone formation with PPA treatment (Fig. 8H). These results suggest that PPA can induce bone formation by promoting osteoblast differentiation in vivo, which then increases bone mass in normal adult mice.

4. Discussion

Marine organisms represent a promising source of biologically active and structurally diverse secondary metabolites and have provided drug leads for the treatment of numerous diseases, especially different forms of cancer. Nevertheless, MNPs also present challenges for drug discovery, such as technical barriers to screening, isolation, characterization, and optimization, which have contributed to a decline in their use for new drug discovery by the pharmaceutical industry from the 1990 s onwards [9]. PPA was first isolated from *Penicillium commune*, in a quantity of 40.7 mg [21]. Five years later, our research group isolated a large amount of PPA (280 mg) from the marine fungus *penicillium solitum* MCCC 3A00215 [12]. The high yield of PPA from *penicillium solitum* indicates its potential for development and application as a candidate drug. In the present study, preliminary screening results of 25 compounds from *Penicillium solitum* MCCC 3A00215 for the ability to induce osteoblast mineralization among BMSCs identified PPA as having this concentration-dependent effect. Accordingly, the present study further explored the anti-osteoporosis activity and mechanism of PPA in vitro and in vivo to elucidate whether PPA could serve as a candidate drug for osteoporosis treatment.

Osteoporosis is a common metabolic bone disease, and treatment is required for the prevention of low bone mass, deterioration of the bone tissue microstructure, and fragility fractures [22]. BMSCs play important roles in regulating the bone regeneration process, and these cells are mobilized and exert reparative effects at sites of bone defects [23]. Aging is known to reduce the number of BMSCs that can differentiate into osteoblasts, which leads to the impairment of bone regeneration and subsequent development of osteogenesis. Thus, a treatment that can direct BMSCs toward osteogenic differentiation could be a viable therapeutic option for bone regeneration and osteoporosis specifically [7]. Consistently, recent studies showed that increasing the ability of BMSCs to differentiate into osteoblasts in aged or estrogen-deficient animal models increases osteogenesis and facilitates new bone formation [24,25]. Currently, very few MNPs have been shown to exert therapeutic effects on osteoblasts, limiting the potential development of such natural compounds for clinical application in osteoporosis treatment [26,27]. In this study, we observed that PPA could promote matrix mineralization in both BMSCs and MC3T3-E1 cells in a dose-dependent manner. In addition, it inhibited the adipogenic differentiation of BMSCs with no significant effect on the chondrogenic differentiation of BMSCs. Gene expression analysis revealed that PPA treatment up-regulated expression of the osteogenesis genes *Runx2*, *Ibsp*, and *Bglap* in BMSCs while inhibiting expression of the adipogenic genes *Pref1*, *Zfp423*, and *Fabp4* (Supplementary Fig. 5 S). Overall, these data showed that PPA can significantly change the differentiation fate of BMSCs to promote osteogenesis. We also observed in this study that PPA stimulated ALP accumulation in an early stage and intracellular calcium deposition at a later stage (Fig. 3B-E). These findings collectively indicate that PPA induces molecular initiation of osteoblastogenesis among both BMSCs and MC3T3-E1 cells.

RNA-seq analysis further revealed alterations in the transcriptome profile of BMSCs treated with PPA. The genes found to be differentially expressed after PPA treatment are significantly enriched in the PI3K-AKT, MAPK, calcium, TNF, and TGF-β signaling pathways. GSK-3β, a critical protein of the "destruction complex", plays roles in the regulation of many upstream signaling pathways, including the AKT signaling pathway. Activation of the AKT signaling pathway can inactivate GSK-3β by phosphorylating Ser9 of GSK-3β, which results in the accumulation and translocation of β-catenin, thereby mediating bone regeneration [20]. The involvement of the AKT/GSK-3β signaling pathway in osteogenesis was investigated by western blot and immunofluorescence staining analyses in this study, and the results showed that PPA up-regulated β-catenin, p-GSK-3β, and p-AKT. (Figs. 5–6). Molecular docking analysis was conducted to further evaluate whether the PPA interacts with the AKT and GSK-3β proteins. The docking results showed that PPA could bind to the ligand binding pockets of AKT and GSK-3β with docking scores of − 5.500 and − 5.057 kcal/mol, respectively, and showed consistency of the binding pockets (Fig. 7). Following its combination with AKT/GSK-3β, PPA possesses the ability to regulate the expression of multiple target genes via the AKT/GSK-3β/β-catenin signaling pathway, thereby augmenting the differentiation and mineralization processes of osteoblasts (Fig. 9).

5. Conclusion

Collectively, our findings illustrate that marine peptide PPA can promote osteoblast differentiation and mineralization by activating AKT/GSK-3β/β-catenin signaling pathways in vitro, leading to the upregulation of *Alpl*, *Runx2*, *Ibsp*, and *Bglap* and downregulation of *HIVEP3*. Moreover, this study revealed the underlying novel mechanism of osteoclastic activation by PPA involves targeting of AKT and GSK-3β. The therapeutic potential of PPA was demonstrated in vivo through the reduction of OVX-induced systemic bone loss. Consequently, PPA, as a natural compound isolated from the deep-sea-derived *Penicillium solitum*, may serve as a potential therapeutic candidate for osteolytic diseases, specifically osteoporosis.

Ethical approval statement

The animal study was reviewed and approved by The Laboratory Animal Management and Ethics Committee of Xiamen University (XMULAC20190084). The experimental procedures adhered to the guidelines outlined in the WMA Statement on animal use in biomedical research, ensuring appropriate experimental design and analysis in the field of pharmacology, as well as those established by a globally acknowledged organization.

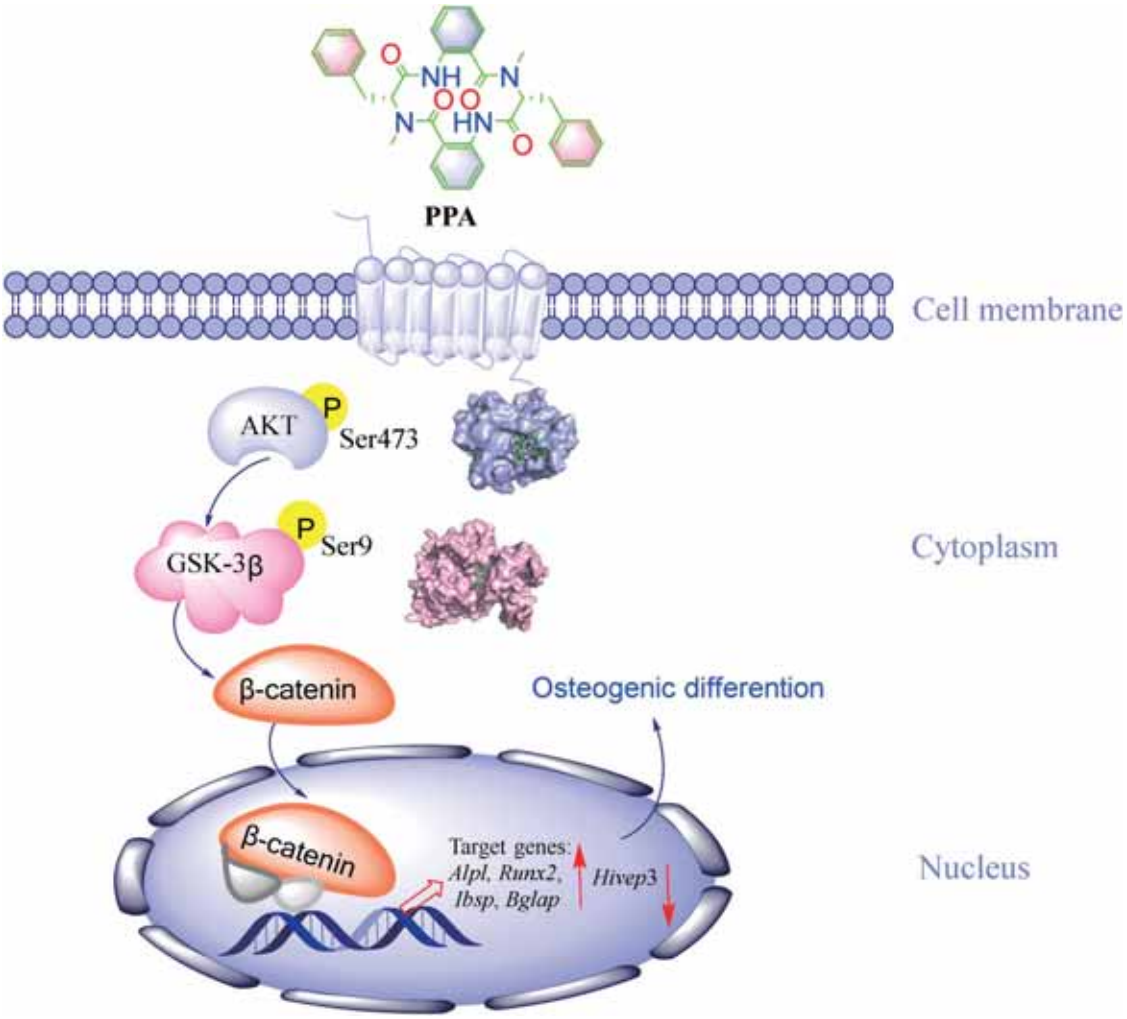

Fig. 9. Schematic diagram of the potential mechanism by which PPA promotes osteoblastogenesis and osteosynthesis by activating the AKT/GSK-3β/β-catenin signaling pathways.

CRediT authorship contribution statement

Chun-Lan Xie performed the research, analyzed data, and wrote the paper. Yu-Ting Yue performed the research and checked the manuscript. Jing-Ping Xu participated part of the experiments (screening of compounds for the ability to induce osteogenic mineralization). The compound PPA was provided by Xian-Wen Yang. Na Li, Ting Lin and Guang-Rong Jie provided material support. Xian-Wen Yang and Ren Xu conceptualized the project and revised the manuscript. All the authors have read and approved the manuscript.

Declaration of Competing Interest

The authors declare that they have no known competing financial interests or personal relationships that could have appeared to influence the work reported in this paper.

Data Availability

Data will be made available on request.

Acknowledgments

This study was supported by the China Postdoctoral Science Foundation (2021TQ0189, 2022M712662), National Natural Science Foundation of China (81972034, 92068104 and 82002262), Xiamen Southern Oceanographic Center Project (22GYY007HJ07), Natural Science Foundation of Fujian Province (2022J06003) and Project of Xiamen Cell Therapy Research (3502Z20214001).

Appendix A. Supporting information

Supplementary data associated with this article can be found in the online version at doi:10.1016/j.phrs.2023.106968.

References

[1] K. Gkastaris, D.G. Goulis, M. Potoupnis, A.D. Anastasilakis, G. Kapetanos, Obesity, osteoporosis and bone metabolism, J. Musculoskel. Neuron 20 (3) (2020) 372–381.
[2] J.M. Patsch, F.W. Kiefer, P. Varga, P. Pail, M. Rauner, D. Stupphann, H. Resch, D. Moser, P.K. Zysset, T.M. Stulnig, P. Pietschmann, Increased bone resorption and impaired bone microarchitecture in short-term and extended high-fat diet-induced obesity, Metabolism 60 (2) (2011) 243–249, https://doi.org/10.1016/j.metabol.2009.11.023.
[3] T.K. Yoo, S.K. Kim, D.W. Kim, J.Y. Choi, W.H. Lee, E. Oh, E.C. Park, Osteoporosis risk prediction for bone mineral density assessment of postmenopausal women using machine learning, Yonsei Med. J. 54 (6) (2013) 1321–1330, https://doi.org/10.3349/ymj.2013.54.6.1321.
[4] Martin, R.B.; Zissimos, S.L.J.B., Relationships between marrow fat and bone turnover in ovariectomized and intact rats. 1991, 12, (2), 123–131, ⟨https://doi.org/10.1016/8756–3282(91)90011–7⟩.
[5] P. Minaire, C. Edouard, M. Arlot, P. Meunier, Marrow changes in paraplegic patients, Calcif. Tissue Int. 36 (1) (1984) 338–340, https://doi.org/10.1007/bf02405340.

[6] G.J. Wang, D.E. Sweet, S.I. Reger, R.C. Thompson, Fat-cell changes as a mechanism of avascular necrosis of the femoral head in cortisone-treated rabbits, J. Bone Jt. Surg. Am. 59 (6) (1977) 729–735, https://doi.org/10.2106/00004623-197759060-00003.
[7] M. Guan, W. Yao, R. Liu, K.S. Lam, J. Nolta, J. Jia, B. Panganiban, L. Meng, P. Zhou, M. Shahnazari, R.O. Ritchie, N.E. Lane, Directing mesenchymal stem cells to bone to augment bone formation and increase bone mass, Nat. Med. 18 (3) (2012) 456–462, https://doi.org/10.1038/nm.2665.
[8] A.R. Carroll, B.R. Copp, R.A. Davis, R.A. Keyzers, M.R. Prinsep, Marine natural products, Nat. Prod. Rep. 39 (2022) 1122–1171, https://doi.org/10.1039/d1np00076d.
[9] A.G. Atanasov, S.B. Zotchev, V.M. Dirsch, C.T. Supuran, Natural products in drug discovery: advances and opportunities, Nat. Rev. Drug Discov. 20 (3) (2021) 200–216, https://doi.org/10.1038/s41573-020-00114-z.
[10] A.H.H. El-Desoky, S. Tsukamoto, Marine natural products that inhibit osteoclastogenesis and promote osteoblast differentiation, J. Nat. Med. 76 (3) (2022) 575–583, https://doi.org/10.1007/s11418-022-01622-5.
[11] Z.H. He, C.L. Xie, T. Wu, Y.T. Yue, C.F. Wang, L. Xu, M.M. Xie, Y. Zhang, Y.J. Hao, R. Xu, X.W. Yang, Tetracyclic steroids bearing a bicyclo[4.4.1] ring system as potent antiosteoporosis agents from the deep-sea-derived fungus *Rhizopus* sp. W23, J. Nat. Prod. 86 (1) (2023) 157–165, https://doi.org/10.1021/acs.jnatprod.2c00866.
[12] Z.H. He, J. Wu, L. Xu, M.Y. Hu, M.M. Xie, Y.J. Hao, S.J. Li, Z.Z. Shao, X.W. Yang, Chemical constituents of the deep-sea-derived *Penicillium* solitum, Mar. Drugs 19 (10) (2021) 580–587, https://doi.org/10.3390/md19100580.
[13] M.M. Beloti, L.S. Bellesini, A.L. Rosa, Purmorphamine enhances osteogenic activity of human osteoblasts derived from bone marrow mesenchymal cells, Cell Biol. Int. 29 (7) (2005) 537–541, https://doi.org/10.1016/j.cellbi.2005.02.007.
[14] F. Faghihi, M. Baghaban Eslaminejad, A. Nekookar, M. Najar, G.H. Salekdeh, The effect of purmorphamine and sirolimus on osteogenic differentiation of human bone marrow-derived mesenchymal stem cells, Biomed. Pharmacother. 67 (1) (2013) 31–38, https://doi.org/10.1016/j.biopha.2012.10.004.
[15] D. Gu, Q. Fan, X. Zhang, J. Xie, A role for transcription factor STAT3 signaling in oncogene smoothened-driven carcinogenesis, J. Biol. Chem. 287 (45) (2012) 38356–38366, https://doi.org/10.1074/jbc.M112.377382.
[16] Z.X. Wang, Z.W. Luo, F.X. Li, J. Cao, S.S. Rao, Y.W. Liu, Y.Y. Wang, G.Q. Zhu, J. S. Gong, J.T. Zou, Q. Wang, Y.J. Tan, Y. Zhang, Y. Hu, Y.Y. Li, H. Yin, X.K. Wang, Z. H. He, L. Ren, Z.Z. Liu, X.K. Hu, L.Q. Yuan, R. Xu, C.Y. Chen, H. Xie, Aged bone matrix-derived extracellular vesicles as a messenger for calcification paradox, Nat. Commun. 13 (1) (2022) 1453–1472, https://doi.org/10.1038/s41467-022-29191-x.
[17] R. Xu, A. Yallowitz, A. Qin, Z. Wu, D.Y. Shin, J.M. Kim, S. Debnath, G. Ji, M. P. Bostrom, X. Yang, C. Zhang, H. Dong, P. Kermani, S. Lalani, N. Li, Y. Liu, M. G. Poulos, A. Wach, Y. Zhang, K. Inoue, A. Di Lorenzo, B. Zhao, J.M. Butler, J. H. Shim, L.H. Glimcher, M.B. Greenblatt, Targeting skeletal endothelium to ameliorate bone loss, Nat. Med. 24 (6) (2018) 823–833, https://doi.org/10.1038/s41591-018-0020-z.
[18] Y. Sun, Q.F. Li, J. Yan, R. Hu, H. Jiang, Isoflurane preconditioning promotes the survival and migration of bone marrow stromal cells, Cell Physiol. Biochem. 36 (4) (2015) 1331–1345, https://doi.org/10.1159/000430300.
[19] D.Q. Wu, W.J. Pan, GSK3: a multifaceted kinase in Wnt signaling, Trends Biochem. Sci. 35 (3) (2010) 161–168, https://doi.org/10.1016/j.tibs.2009.10.002.
[20] D.Y. Zhu, B. Lu, J.H. Yin, Q.F. Ke, H. Xu, C.Q. Zhang, Y.P. Guo, Y.S. Gao, Gadolinium-doped bioglass scaffolds promote osteogenic differentiation of hBMSC via the Akt/GSK3β pathway and facilitate bone repair in vivo, Int. J. Nanomed. 14 (2019) 1085–1100, https://doi.org/10.2147/ijn.S193576.
[21] W. Sun, X. Chen, Q. Tong, H. Zhu, Y. He, L. Lei, Y. Xue, G. Yao, Z. Luo, J. Wang, H. Li, Y. Zhang, Novel small molecule 11beta-HSD1 inhibitor from the endophytic fungus *Penicillium commune*. Sci. Rep. 6 (2016) 26418–26427, https://doi.org/10.1038/srep26418.
[22] Z.F. Zhao, M. Nian, H. Lv, J.X. Yue, H.F. Qiao, X.H. Yang, X.H. Zheng, Advances in anti-osteoporosis polysaccharides derived from medicinal Hherbs and other edible substances, Am. J. Chin. Med. 50 (02) (2022) 441–470, https://doi.org/10.1142/s0192415x22500173.
[23] F. Yang, D. Yang, J. Tu, Q. Zheng, L. Cai, L. Wang, Strontium enhances osteogenic differentiation of mesenchymal stem cells and in vivo bone formation by activating Wnt/catenin signaling, Stem Cells 29 (6) (2011) 981–991, https://doi.org/10.1002/stem.646.
[24] M. Bonyadi, S.D. Waldman, D. Liu, J.E. Aubin, M.D. Grynpas, W.L. Stanford, Mesenchymal progenitor self-renewal deficiency leads to age-dependent osteoporosis in Sca-1/Ly-6A null mice, Proc. Natl. Acad. Sci. USA 100 (10) (2003) 5840–5845, https://doi.org/10.1073/pnas.1036475100.
[25] O. Katsara, L.G. Mahaira, E.G. Iliopoulou, A. Moustaki, A. Antsaklis, D. Loutradis, K. Stefanidis, C.N. Baxevanis, M. Papamichail, S.A. Perez, Effects of donor age, gender, and in vitro cellular aging on the phenotypic, functional, and molecular characteristics of mouse bone marrow-derived mesenchymal stem cells, Stem Cells Dev. 20 (9) (2011) 1549–1561, https://doi.org/10.1089/scd.2010.0280.
[26] X. Wang, K. Yamauchi, T. Mitsunaga, A review on osteoclast diseases and osteoclastogenesis inhibitors recently developed from natural resources, Fitoterapia 142 (2020) 104482–104493, https://doi.org/10.1016/j.fitote.2020.104482.
[27] S.R. Chaugule, M.M. Indap, S.V. Chiplunkar, Marine natural products: new avenue in treatment of osteoporosis, Front. Mar. Sci. 4 (2017) 384–398, https://doi.org/10.3389/fmars.2017.00384.